BEN GURION UNIVERSITY OF THE NEGEV
FACULTY OF ENGINEERING SCIENCES
DEPARTMENT OF INDUSTIRLA ENGINEERING AND MANAGMENT

BAYESIAN ESTIMATION OF SPATIAL CONFIGURATION DISTRIBUTION

THESIS SUBMITTED IN PARTIAL FULFILLMENT OF THE REQUIRMENETS
FOR THE M.Sc. DEGREE

By: Rotem Duani

OCTOBER 2017

BEN GURION UNIVERSITY OF THE NEGEV
FACULTY OF ENGINEERING SCIENCES
DEPARTMENT OF INDUSTIRLA ENGINEERING AND MANAGMENT

BAYESIAN ESTIMATION OF SPATIAL CONFIGURATION DISTRIBUTION

THESIS SUBMITTED IN PARTIAL FULFILLMENT OF THE REQUIRMENETS
FOR THE M.Sc. DEGREE

By: Rotem Duani

Supervised By: Prof. Sigal Berman

Author:………………………………………………………… Date:…………..

Supervisor:…….……………………………………………. Date:…………..

Chairman of Graduate Studies Committee:………………… Date:…………..

OCTOBER 2017

Abstract

Grasping and manipulating objects in dense un-structured environments is challenging both for humans and for robotic systems. One of the essential components of a successful grasp, is the position and orientation (pose) of the wrist, from which the object is grasped. Determining such a goal pose is an important part of reach-to-grasp motion planning. Grasp affordance densities are spatial probability density functions that represent grasp success probability from wrist poses about the object. To represent both position and orientation well, the density function must be based on a mixture model which includes both cyclic and non-cyclic components. We developed a non-parametric Bayesian estimation method suitable for a mixture of such combined density functions composed of Gaussian and Von-Misses-Fisher functions. Non-Parametric Bayesian estimation facilitates joint estimation of both mixture component, number and component parameters and is less prone to being trapped in local minima, or to over-fitting the dataset, than maximum likelihood based estimation methods. The developed method is incorporated in a reach-to-grasp motion planning algorithm and is applied to motion analysis in patients with stroke. For reach-to-grasp motion planning, we integrated the grasp affordance density estimation with bi-direction Randomly exploring Random Tree (RRT) motion planning algorithm. The developed algorithm, grasp affordance-RRT (GA-RRT) facilitates multiple goal configurations with a high grasp success probability. The GA-RRT algorithm was tested in simulation for motion planning towards a mug in five different environments with obstacles. In one of the environments, the algorithm did not find suitable goal configurations, since it was very cluttered and required approach orientations that were not included in the original data-base from which the density was estimated. In the other four environments, 95% of trials led to successful grasps. The grasp affordance estimation method was applied for estimating affordance densities of 15 patients with stroke and 13 healthy, aged-matched controls. Subjects in both groups performed reach-to-grasp movements towards four targets locations. A grasp affordance density was estimated for each group with data from all targets combined. For both groups the estimated densities comprised two components, yet the division of grasp configurations between the components in each density mixture, differed between the groups. For the health group, the configurations of three target locations were allocated to one density mixture component and one target was allocated to a separate component. For the stroke group, subjects were divided between the components based on the effected arm, with which they performed the motion. In addition, the variance of the density components was much higher for the stroke group.

Key words: non-parametric Bayesian estimation, Grasp affordance density, Gaussian Mixture Model, Von Mises-Fisher distribution, Grasping, Motion planning, Stroke.

ACKNOWLEDGMENTS

I would like to thank my academic advisor, Prof. Sigal Berman, for continuously supporting my research, for her endless patience, dedication and professional guidance. I learnt a lot from this process and I owe that to you.

A great thanks to Dr. Yoav Kerner for the constant assistance with analysis and professional statistical guidance. Thanks to Prof. Dario G. Liebermann and Dr. Mindy F. Levin for their professional support and advise. I would also like to thank Isgav Davidowitz for his friendly and professional support.

Furthermore, thanks to Silvi Frenkel-Toledo, Melanie C. Baniña, Dr. Nachum Soroker, Dr. John M. Solomon, Isgav Davidowitz and Akash Shah for their assistance with the data collection.

The project is supported by the Canada-Israel Binational cooperation (MFL, DGL) Joint Canada-Israel Health Research Program, funded by the Israel Science Foundation (ISF) grant number 2392\15, the Azrieli foundation, the Canadian Institutes of Health Research (CIHR), the International Development Research Center (IDRC) grant number 108186-001, and the Helmsley Charitable Trust through the Agricultural, Biological and Cognitive Robotics Center of Ben-Gurion University of the Negev.

Table of Contents

Abstract 2

Table of Contents 5

List of Figures 7

List of Tables 9

Acronyms 10

1. Introduction 11

1.1. Background 11

1.2. Goals and Innovation 12

1.3. Research scope and limitations 13

1.4. Thesis outline 13

2. Literature review 14

2.1. Overview 14

2.2. Theoretical foundations 14

2.2.1. Cyclic distribution functions 14

2.2.2. Mixture models 15

2.3. A Non-Parametric Bayesian estimation method for GMMs 21

2.4. Robotic reach-to-grasp motion 22

2.5. Reach-to-grasp motion of patients with stroke 25

3. Non-parametric Bayesian estimation of grasp affordance 27

3.1. Overview 27

3.2. Non- parametric Bayesian estimation algorithm description 27

3.3. Validation experiment 31

3.3.1. Data 31

3.3.2. Experimental protocol 32

3.3.3. Results 32
3.3.4. Discussion 42
4. Robotic reach-to-grasp motion planning 44
4.1. Overview 44
4.2. GA-RRT algorithm 44
.4.3 Experiment 46
4.3.1. Object and Environment 46
4.3.2. Experimental protocol 47
4.3.3. Analysis 47
4.4. Results 48
4.5. Discussion 52
5. Analysis of reach-to-grasp motion of patients with stroke 53
5.1. Overview 53
5.2. Method 53
5.2.1. Subjects 53
5.2.2. Environment 54
5.2.3. Experimental Protocol 55
5.2.4. Analysis 55
5.3. Results 56
5.3.1. Grasp affordance density of healthy subjects 56
5.3.2. Grasp affordance density of patients with stroke 58
5.4. Discussion 60
6. Bibliography 62
Appendix 1: Synthetic data sets 66
Appendix 2: Demographic data 68

List of Figures

Figure 2.1: VMF distribution in 3D space 15
Figure 2.2: Parametric Vs Non-Parametric Visualization 18
Figure 2.3: Non-parametric Bayesian estimation- flow chart 21
Figure 2.4: Adding a new node to an existing graph (Lavalle 2006) 23
Figure 2.5: Dealing with an obstacle to prevent collision 24
Figure 2.6: GR-RRT algorithm 25
Figure 3.1: Non-parametric Bayesian estimation algorithm – flow chart **שגיאה! הסימניה אינה מוגדרת.**27
Figure 3.2: Position only- mixture model 33
Figure 3.3: Position only - distribution by component 33
Figure 3.4: Orientation only- mixture model and convergence 34
Figure 3.5: Orientation only - distribution by component 34
Figure 3.6: Integrated algorithm- mixture model and convergence 35
Figure 3.7: Integrated algorithm- distribution by component 35
Figure 3.8: Position overlap - samples generated 36
Figure 3.9: Position overlap- convergence and mixture model 37
Figure 3.10: Position overlap – distribution by component 37
Figure 3.11: Orientation overlap- samples generated 38
Figure 3.12: Orientation overlap – convergence and mixture model 39
Figure 3.13: Orientation overlap - distribution by component 39
Figure 3.14: Total overlap - samples generated 40
Figure 3.15: Total overlap-convergence and mixture model 41
Figure 3.16: Total overlap- distribution by component 41
Figure 4.1: GA-RRT - Run time planning phase Flow chart ..... 44**שגיאה! הסימניה אינה מוגדרת.**
Figure 4.2: Mug's dimensions 46
Figure 4.3: Grippers dimensions 46
Figure 4.4: Grasps generated by expert 46

Figure 4.5: The physical environment in the telerobotic laboratory 47
Figure 4.6: The five environment compositions 47
Figure 4.7: Mug convergence and mixture model .... 48.שגיאה! הסימניה אינה מוגדרת
Figure 4.8: Mug distribution by component 49
Figure 4.9: Environment 1- representative grasps 50
Figure 4.10: Environment 2- representative grasps 51
Figure 4.11: Environment 3- representative grasps 51
Figure 4.12 : Environment 4- representative grasps 51
Figure 5.1: Cones for grasp 54
Figure 5.2 : Experimental setup 54
Figure 5.3 : G4 tracking system 54
Figure 5.4: Segmentation analysis graph 56
Figure 5.5: Healthy subjects- distributions by cluster 57
Figure 5.6: Healthey subjects- convergence and mixture model 57
Figure 5.7: Healthy subjects- Component composition by target שגיאה! הסימניה אינה מוגדרת.60
Figure 5.8: Patients with stroke- convergence and mixture model 58
Figure 5.9: Patients with stroke - distribution by component 59
Figure 5.10: Patients with stroke- Component composition by target 59

List of Tables

TABLE 1 : Parameters and hyper parameters' distributions 28
TABLE 2: Position only- parameters per cluster 33
TABLE 3: Orientation only-parameters per component 34
TABLE 4: Integrated algorithm - parameters per component 36
TABLE 5: Position overlap -parameters per component 38
TABLE 6: Orientation overlap- parameters per component 40
TABLE 7: Total overlap- parameters per component 42
TABLE 8: Parameter initiation 43
TABLE 9: Mug-Parameters per component 49
TABLE 10: Average results per environment 50
TABLE 11: Healthy subjects- mixture model parameters 58
TABLE 12: Patients with stroke- mixture model parameters 59
TABLE 13: The dominant cluster of patients with stoke 60

Acronyms

ARS	Adaptive rejection sampling
BIC	Bayesian Information Criterion
EM	Expectation Maximization
DOF	Degrees-of-Freedom
ENHANCE	Enhancing brain plasticity for sensorimotor recovery in spastic hemiparesis
FC	Far Centre
FL	Far Left
FR	Far Right
GARRT	Grasp Affordance Rapidly exploring Random Trees
GMM	Gaussian Mixture Model
GRRRT	Grasp Range Rapidly exploring Random Trees
ICL	Integrated Completed Likelihood
IGMM	Infinite Gaussian Mixture Model
KDE	Kernel Density Estimation
NC	Near Center
OP	Overlap Position dataset
OO	Overlap Orientation dataset
OPO	Overlap in Position and Orientation dataset
RRT	Rapidly exploring Random Trees
SE	Special Euclidian
TCP	Tool Center Point
VMF	Von Misses-Fisher
WGR	Workspace Goal Regions

1. Introduction

1.1. Background

Grasping is a fundamental skill needed by both humans and robots for object manipulation, and involves both hand and arm motion. For performing a required grasp, the arm must reach a final wrist configuration in task space and the fingers must reach required contact points on the object. Based on available degrees of freedom, arm and finger joint configuration should also be determined. In the current research, we focus on grasp wrist configurations in task space. Wrist configurations are composed of six parameters, where three parameters represent the position (X, Y, Z) and three parameters represent the orientation (σ, θ, ϕ). They can be represented in object-centered coordinates, which facilitates defining grasp configurations based on gripper and object without regard to the environment in which the object is placed.

Grapability maps have been used to store quality grades for object centered, grasp wrist configurations (Eizicovits and Berman 2014). They can be used to generate grasp affordance densities (Detry et al. 2009), which are spatial probability density functions that represent grasp success probability for wrist configurations about the object. Grasp affordance densities are typically mixture models composed of both, Gaussian and cyclic components, used for representing position and orientation respectively (Detry et al. 2009). Previous methods employed for estimating distribution parameters, include Expectation Maximization (EM) (Granville, Fagg, and Southerland 2006) and Kernal Density Estimation (KDE) (Detry et al. 2009). In contrast, the current work investigated the use of non-parametric Bayesian estimation.

There are two main approaches for statistical inference, maximum likelihood (Frequentist) and Bayesian. The Bayesian approach uses Bayes' theorem to combine observational data with prior knowledge, not expressed in observations, (Press 2002). While, the frequentist approach assumes that the sampled data is representative, and a subjective prior may cause bias. One of the main advantages of the Bayesian approach are that data can be used as it comes in. There is no requirement that every contingency be planned for ahead of time, very useful in machine learning and big Data methods(Orloff and Bloom 2014). In this work we explore the Bayesian approach in the grasp affordance estimation method.

1.2. Goals and Innovation

This research presents a non-parametric Bayesian estimation method which generates grasp affordance densities. The algorithm jointly estimates component parameters, mixture weight, and the number of mixture components. The algorithm developed is suitable for estimation of a mixture model composed of Von Mises-Fisher (VMF) and Gaussian distributions components. It integrates two estimation algorithms, the Infinite Gaussian Mixture Model (Rasmussen 2000) and Infinite VMF Mixture Model (Bangert 2010). The development required adaptation of sampling algorithms due to numeric issues, adaptation of priors and hyper parameters estimators, determination of parameter hierarchy levels and normalization of Gaussian and VMF likelihood probabilities. The grasp affordance density was incorporated in a robotic motion planning algorithm and used for analysis of motion in patients with stroke.

We developed the Grasp Affordance Randomly exploring Random Tree (GA-RRT) algorithm based on the Grasp Region Randomly exploring Random Tree (GR-RRT) algorithm (Reshef, Eizicovits, and Berman 2014). The modifications included, the development and integration of a suitable mixture model random sampling algorithm. The GA-RRT algorithm provides high quality target configurations resulting in greater likelihood of successful grasps.

The analysis of motion of patients with stroke was done as part of the ENHANCE project. The goal of ENHANCE is to establish and clinically validate effective upper limb interventions for recovery of voluntary movement control after stroke. Human grasp configurations of both healthy subjects and patients with stroke were evaluated. Two separate grasp affordance densities were generated, one for each group for motion towards four targets. Analysis of the grasp affordance densities included comparison of the number of clusters, composition of clusters and variance within clusters. By analyzing these measures, we can learn about the number of grasp types and the difference between them. For both groups the estimated densities comprised two components, yet the division of grasp configurations between the components in each density mixture, differed between the groups. For the control group, the configurations of three target locations were allocated to one density mixture component and one target was allocated to a separate component. For the stroke group, subjects were divided between the components based on the effected arm, with which they performed the motion. In addition, the variance within the components was much higher for the stroke group.

1.3. Research scope and limitations

The current research revolves around the Bayesian distribution estimation method, testing its limits, using it for modifying a path planning method evaluated in simulation, and for the analysis of the motion of patients with stroke. One direction for future research involves further examination of the estimation algorithm by examining optimization of currently, constant, hyper parameters, and providing the option of using previous grasp affordance densities as the prior. For the path planning algorithm, further examination with hardware and comparison to other existing algorithms. For the motion of patients with stroke, examining the post treatment and follow-up data of patients and analyze the progress made throughout the treatment is left to future research, as the ENHANCE project is still in-process and the data is not yet available.

1.4. Thesis outline

This thesis is organized as follows: chapter 2 presents a literature review of the basic concepts and methods, various distribution estimation algorithms are explained, existing, commonly used, motion planning algorithms are presented, and impairment in grasping of patients with stroke is explained. Chapter 3 includes a detailed description of the algorithm developed, and the results of synthetic data used for validation. In chapter 4, an implementation of the algorithm in robotic path planning is presented and analyzed. Finally, in chapter 5, an implementation of the algorithm on post stroke grasp data is presented and analyzed.

2. Literature review

2.1. Overview

This chapter includes the review of different concepts and methods, related to non-parametric Bayesian estimation of grasp affordance densities and the use of such affordance estimation in robotic motion planning and human motion analysis. Theoretical statistical foundations are presented in section 2.1. These include cyclic distributions, mixture models, and three algorithms used for estimating grasp affordance densities which are reviewed and compared. Section 2.2 briefly presents Rapidly exploring Random Trees (RRT) motion planning algorithms. Section 2.3 describes reach-to-grasp characteristics in healthy subjects and in patients with stroke.

2.2. Theoretical foundations

2.2.1. Cyclic distribution functions

There are various practical situations in which observations include orientations, e.g. the orientation from which to grasp an object. In such cases spherical statistics is required for handling the angular data. Cyclic distributions are a tool offered by spherical statistics for expressing the periodic characteristics of angles.

Using quaternion representation is common in cyclic distributions. Quaternions are used to express an orientation of a point in 3D space around an axis. They are composed of four components (q_0, q_1, q_2, q_3), where q_0 represents a scalar and (q_1, q_2, q_3) represent a vector. Quaternions and Euler angles both represent orientation, however using quaternions has several advantages, such as easier conversion to orientation matrices and avoidance of and gimbal lock. In addition, when using quaternions, the order of orientation doesn't need to be specified like in Euler angles. The functional linkage between Euler angles and quaternions is:

$$q_0 = \cos\left(\frac{\alpha}{2}\right), \qquad q_1 = \sin\left(\frac{\alpha}{2}\right)\cos(\beta_x), \qquad q_2 = \sin\left(\frac{\alpha}{2}\right)\cos(\beta_y), \qquad q_3 = \sin\left(\frac{\alpha}{2}\right)\cos(\beta_z)$$

Where α is orientation angle (the value in radians of the angle of orientation), and $\cos(\beta_x)$, $\cos(\beta_y)$ *and* $\cos(\beta_z)$ are the direction cosines locating the axis of orientation.

2.2.1.1. Von-Mises Fisher (VMF) distribution

The Von Mises - Fisher (VMF) distribution is a commonly used cyclic distribution, as it is the equivalent of the Gaussian distribution in the cyclic world (Figure 2.1). The VMF distribution has two parameters: μ, the expected value, and *kappa*, the concentration of the data.

A p-dimensional unit random vector $\bar{X}$ ($||\bar{X}|| = 1$) with a p-variate VMF distribution, has a probability density function (pdf):

$$f(x|\mu, kappa) = c_p(kappa)e^{\,kappa * \mu^{T} x} \quad (1)$$

Where $||\mu|| = 1, kappa \geq 0$, and $c_p(kappa)$ the normalizing constant is given by:

$$C_p(kappa) = \frac{kappa^{\frac{p}{2}-1}}{(2\pi)^{\frac{p}{2}} I_{\frac{p}{2}-1}(kappa)} \quad (2)$$

As *kappa* decreases the pdf becomes more similar to a uniform pdf (Dhillon and Sra 2003).

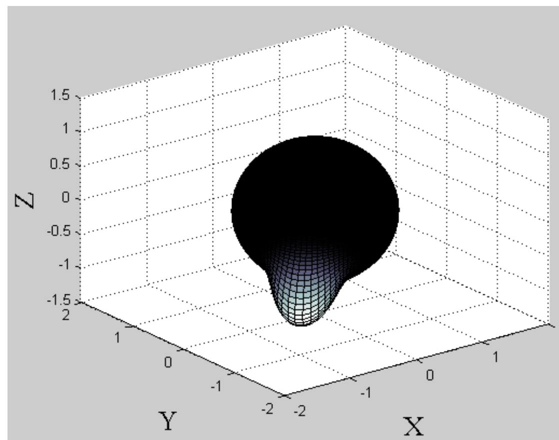

Figure 2.1: VMF distribution in 3D space

2.2.2. Mixture models

A mixture model is a probabilistic model used for representing subpopulations within an overall population. Mixture models are used to make statistical inferences about the properties of the sub-populations, given observations on the pooled population, this without sub-population identity information (Everitt 1981). The mixture model assumes the existence of M densities, where each density is allocated a weight value, and the sum of all weights adds to 1 (Reynolds 2008). When fitting a mixture model to data, the mixture weight and component parameters are determined (Reynolds 2008). The Gaussian Mixture Model (GMM) is a broadly used model in which all M densities are Gaussian. GMM has been used in many fields, e.g., for modeling vocal-tract related spectral features in a speaker recognition system (Reynolds 2008), human skin colors for security checks (Yang and Ahuja 1998), acoustic units for speech recognition (Torbati, Picone, and Sobel 2013). An example for the probabilistic mixture model follows:

$$g(x|\Theta) = \sum_{i=1}^{k} w_i P_i(x|\theta_i) \tag{3}$$

Where x represents the independent identically distributed samples, θ_i, are the parameters of $cluster_i$'s distribution and w_i represents the weight of mixture 'i'. Parameters of mixture models cannot be directly estimated using the classical maximum likelihood estimators, there are several ways to estimate the parameters of a mixture model: Expectation Maximization (EM) (Reynolds 2008), Kernel Distribution Estimation (KDE), and non-parametric Bayesian Estimation.

2.2.2.1. Expectation Maximization (EM)

The EM algorithm is an iterative method for finding maximum likelihood or maximum posteriori estimates of parameters, where the model depends on latent variables. EM operates in two phases. First, E-Step, computes the probability of given samples to belong to the different clusters. Second, set the parameters of the clusters (θ) to maximize the log likelihood function (equation 5) (Xu and Jordan 1996):

$$E(l(\theta)) \ = \mathrm{E}(Log(\prod_{i=1}^{N} P(x_i|\,\theta)) = \mathrm{E}(\sum_{i=1}^{N} Log(p(x_i|\,\theta))) \tag{5}$$

Where θ indicates the estimated parameters and x represents a d dimensional sample. The EM algorithm will attempt to optimize the expression $E(l(\theta))$ repeating the two phases described above until reaching convergence or a-priori determined number of repetitions. Using the EM algorithm, to estimate a Gaussian distribution follows (Xu, Jordan, and Hinton 1994). The E step, computes:

$$h_j{}^{(k)}(i) = \frac{w_j{}^{(k)} P(x^{(i)}|\mu_j{}^{(i)}, \Sigma_j{}^{(i)})}{\sum_{t=1}^{M} w_t{}^{(k)} P(x^{(i)}|\mu_t{}^{(i)}, \Sigma_t{}^{(i)})} \tag{6}$$

The M step, finds a new estimate for parameters $\theta = \{w_j, \mu_j, \Sigma_j\}$ using equations 7-9.

$$w_j{}^{(k+1)} = \frac{\sum_{i=1}^{D} h_j{}^{(k)}(i)}{N} \tag{7}$$

$$\mu_j{}^{(k+1)} = \frac{\sum_{i=1}^{D} h_j{}^{(k)}(i) x^{(i)}}{\sum_{i=1}^{D} h_j{}^{(k)}(i)}$$

(8)

$$\Sigma_j{}^{(k+1)} = \frac{\sum_{i=1}^{D} h_j{}^{(k)}(i) \left[x^{(i)} - \mu_j{}^{(k)}\right]\left[x^{(i)} - \mu_j{}^{(k)}\right]^T}{\sum_{i=1}^{D} h_j{}^{(k)}(i)}$$

(9)

Where w_j indicates the weight of component 'j', the mean vectors are represented by μ_j, and the covariance matrices $\sum_j$. In the EM algorithm, the number of components is set a-priori. To find the most suitable model, given the number of components is not known, the algorithm is repeated several times with a different number of clusters. The best model is determined using statistical criterion indicator. Two common statistical criterions are the Bayesian information criterion (BIC) and the Integrated Completed Likelihood (ICL).

The Bayesian Information Criterion (BIC) was developed as an approximation to the log marginal likelihood of a model, and therefore, the difference between two BIC estimates may be a good approximation to the natural log of the Bayes factor (Posada and Buckley 2004). Choosing the model with the smallest BIC is equivalent to selecting the model with the maximum posterior probability. The BIC is formally defined as

$$BIC = \mathrm{k} * \ln(n) - 2\ln(\hat{L})$$

(10)

Where $\hat{L}$ is the maximized value of the likelihood function of the model M i.e. $\hat{L} = p(x|\hat{\theta}, M)$ where $\hat{\theta}$ are the parameter values that maximize the likelihood function, x is the observed data, n is the sample size and k is the number of free parameters to be estimated. The BIC criterion suffers from three main limitations: the approximation is only valid for sample size n much larger than the number of parameters, k in the model, the BIC cannot handle complex collections of models, as in the variable selection problem in high-dimension and it often over estimates the number of clusters (Posada and Buckley 2004).

Like the BIC, Integrated Completed Likelihood (ICL) prefers models which explain the training data and punish complexity. The ICL criterion, gives an answer to the tendency of BIC to overestimate the number of clusters. This is done by replacing the maximum a posteriori probability estimator of a sample x_i to belong to a cluster k with the missing cluster indicators z_{ik} (Itti, Koch, and Niebur 2010):

$$z_{ik} = \begin{cases} 1 - \text{ if } \arg\max(\hat{\theta}) = k \\ 0 - otherwise \end{cases}$$

(10)

2.2.2.2. Kernel Density Estimation

Kernel Density Estimation (KDE) estimates non-parametric models. A non-parametric model, does not assume a fixed number of parameters. As the number of samples grows the number of parameters grows. In parametric models, the goal is to model the data in the best way, given a known number of clusters. For example, in Figure 2.2A, a parametric model is presented, the model attempts to fit one cluster to all observations in the best way possible. In non-Parametric models (Figure 2.2B), each sample can be represented by a cluster. Some samples will merge (after smoothing) to represent one cluster. Theoretically, enabling the model to have a cluster per sample (Detry et al. 2009).

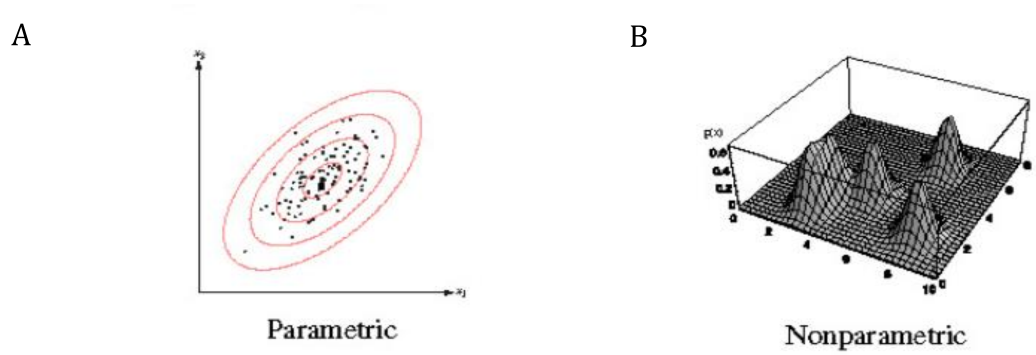

Figure 2.2: Parametric Vs Non-Parametric Visualization

2.2.2.3. Bayesian estimation

Bayesian estimation is based on Bayes' rule:

$$P(H|D) = \frac{P(D|H)P(H)}{P(D)}$$

(11)

Where H and D are events and P(D)≠0. An additional interpretation is available, where H is a hypothesis and D is data which may give evidence for or against H. The prior P(H) is the probability that H is true before the data is considered. The posterior P(H|D) is the probability that H is true after the data is considered. The likelihood P(D|H) is the evidence about H provided by the data D. P(D) is the total probability of the data considering all possible hypotheses (Orloff and Bloom 2014). In most experiments, the prior probabilities on hypotheses are not known. Thus, priors can be determined using trial and error or maximum likelihood methods.

Each observation is composed of some pattern (in distribution estimation the parameters of the distribution is the pattern and their values are the hypothesis (H)) plus an independent noise. Assuming the observations are independent and identically distributed (IID) is required, however in this case it is clear the observations are not IID, they are conditionally independent (Gelman et al. 2014). Conditional independence means that given the parameter information the data is independent, identically distributed and exchangeable (changing the order in which the data was entered does not change the joint distribution). Conditional independence is sufficient according to de Finety (de Finetti 1995)

The prior P(H) is previous information we have or assume about the model. In case there is no prior knowledge, it is common to either guess or use the likelihood. Conjugate priors are commonly used when estimating distributions as using them generates analytical equations (Murphy 2007). For example, the weight parameters of a mixture model are distributed multinomial as they are positive numbers which add to one therefore their conjugate prior is the Dirichlet distribution where α *and* G_0 represent the priors in the Dirichlet distribution (Ferguson 2014).

2.2.2.4. Comparison of model estimation methods

The EM estimation requires prior information regarding both the type of distribution as well as the number of components examined. When using the EM algorithm, we are prone to over-fitting as an optimization to the data is performed. Additionally, initial values influence the results and we may encounter local minima. Granville and Fagg (Granville, Fagg, and Southerland 2006), generated grasp affordance densities using EM estimation along with model selection criteria for mixture-model parameter estimation, trying to identify representative components.

KDE, on the other hand, is an algorithm which initially represents each sample with a cluster, causing high dimensionality. Thus, attempting to compute an analytical equation to model the distribution is very complicated, time consuming and often, impossible (Shalizi 2016). Detry, (Detry et al. 2009) applied kernel-density estimation methods for vision based grasp learning successfully.

When using the non-parametric Bayesian estimation, the number of clusters is among the estimated parameters and need not be set a-priori. Additionally, the use of conjugate priors derives, easily computed, analytical equations (describing the distribution). Furthermore, the parameters are drawn at each iteration, thus marginalizing over all possibilities.

2.3. A Non-Parametric Bayesian estimation method for GMMs

A non-parametric Bayesian estimation method for infinite GMMs was suggested by Rasmussen (2000). It has been successfully implemented for examining neuron signals.

The algorithm works as follows (Figure 2.3), first, priors are generated using maximum likelihood estimators. During algorithm initiation, the priors are calculated given that all observations belong to a single cluster. Second, the parameters and hyper parameters of clusters are sampled, using the conditional posterior distributions and the Gibbs sampler. The Gibbs sampler is a technique for generating random variables from a marginal distribution indirectly, without having to calculate the density (Casella and George 1992).

Once the parameters and hyper parameters of each cluster are sampled, a new cluster is sampled for each observation. This is also done using the Gibbs sampler, where the conditional posterior distributions depend on the parameters of the cluster the observation was last allocated to. The clusters sampled for each observation now pose an alternative for the current cluster the observation is allocated.

The probability for each observation to originate from an existing cluster or a new cluster is estimated using the Dirichlet Process Posterior:

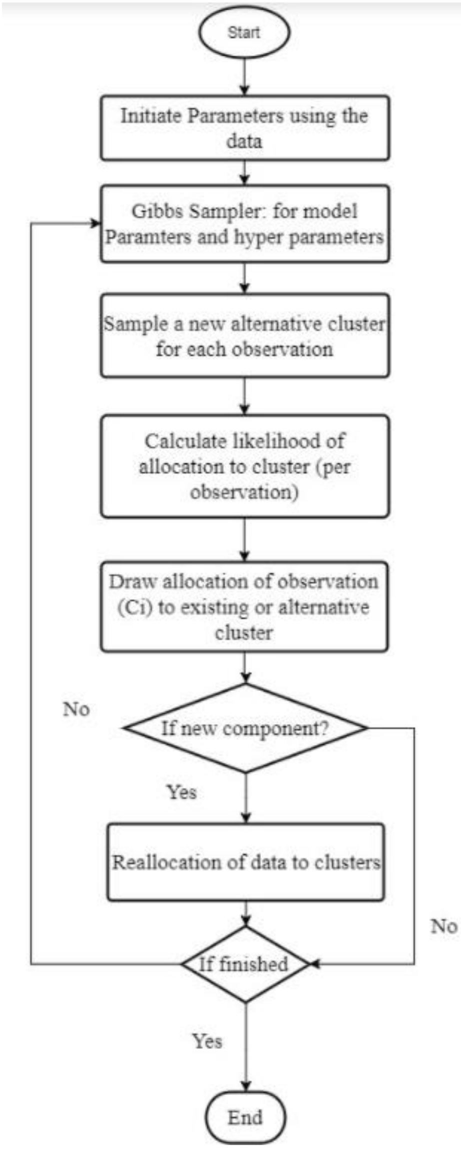

Figure 2.3: Non-parametric Bayesian estimation- flow chart

$$\theta_{n+1}|\theta_1,\ldots,\theta_n \sim \frac{1}{n+\alpha}\sum_{j=1}^{n}\delta_{\theta_j}(\theta_{n+1}) + \frac{\alpha}{n+\alpha}G_0(\theta_{n+1}) \tag{12}$$

$$p(x_{n+1}|x_1,\ldots,x_n) = \sum_{k=1}^{K_n}\frac{n_k}{n+\alpha}p(x_{n+1}|\theta_k^*) + \frac{\alpha}{n+\alpha}\int p(x_{n+1}|\theta)G_0(\theta)d\theta \tag{13}$$

Where θ represents the parameters of a specific cluster, n is the number of samples and x represents the observations. The estimation in equation 12 will be used and inserted into equation 13. We can now sample using equation 13, the probability that the data point has originated from an already existing cluster (first expression in equation 13), and the probability that it is a new cluster (the second expression in the equation). Once a new cluster is proposed the probability of each data point to belong to the new cluster (likelihood) is calculated. The new cluster is now proposed to all data observations, the decision to belong to the new cluster does not depend solely on the likelihood, the likelihood is used as input to the multinomial distribution. At each iteration, for each data point a multinomial allocation is drawn and the allocation to cluster is determined (C_i indicates the cluster allocation for observation i). To conclude, at different iterations a data point may be affiliated with one cluster and at the following iteration it may belong to another.

Each iteration generates a valid estimation of the distribution model. However, to reach convergence and stable allocation of observations, many iterations need to be executed. To reduce complexity and computation time, at each iteration only one new cluster can be proposed to all observations (Mandel 2005).

2.4. Robotic reach-to-grasp motion

To successfully grasp and manipulate an object, a robot must bring its end-effector to a pose (position and orientation) from which a high-quality grasp can be formed. When the object to be grasped is known, grasps (end-effector configurations) can be synthesized a-priori. When the object location with respect to the manipulator is additionally known, manipulator grasp poses and configurations can additionally be computed a-priori. A collision-free path to a grasp configuration can be computed a-priori only in a known, static environment.

The path planning problem is the robot's attempt to plan the arrival to its target position while avoiding obstacles along the way. Given a starting position, a target position and obstacles a path planning algorithm attempts to find a continues path while avoiding collisions. The common procedures for motion planning are executed in iterations, in each iteration, an attempt is made to advance towards the target position. If the attempt is successful, then it will be made otherwise another move will be examined.

There are many algorithms for motion planning available. Many motion planning algorithms resembles the problem to sampling and searching t possibilities trees. Such as the Rapid Exploring Random Tree (RRT) and its variants (Lavalle 2006).

RRT is used frequently due to its efficiency and ability to deal with constraints. RRT belongs to the Rapidly Exploring Dense Trees (RDT) family and differs from other sample and search algorithms in its ability to gradually improve its space coverage. The tree will eventually, densely cover the space (Lavalle 2006).

RRT algorithm attempts to find a free-collision path from the origin (q_0) to the goal (q_{goal}) using a sequence of random samples (where a_i is the i^{th} sample). In each iteration a_i is connected to the graph (at point q_n) via the shortest path. If q_n is a vertex, then it connects an edge between the two ($a_i$and q_n). Otherwise if q_n is an edge, α_i's connection to the graph will generate two new vertices (the second one being the point on the edge where $a_i$was connected) (Figure 2.4).

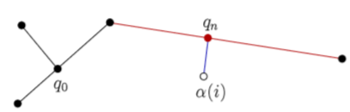

Figure 2.4: Adding a new node to an existing graph (Lavalle 2006)

When the path between a_i and q_n is not feasible due to the presence of an obstacle, an edge will be made from q_n to q_s (q_s being the last point possible before hitting the obstacle). The closeness of q_s to the obstacle depends on both the algorithm chosen to check for collision as well as the algorithm chosen to find the nearest point (exact or approximate) (Figure 2.5).

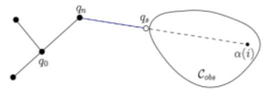

Figure 2.5: Dealing with an obstacle to prevent collision

Single tree search uses the algorithm above to expand the tree from q_0. In each iteration, the algorithm will either select $a_i$or q_{goal} and check whether it is possible to connect the RRT to the q_{goal}. The selection between a_i and q_{goal} can be implemented in different ways.

The balanced, bidirectional search method usually outperforms the single tree search. The search produces two RRT trees. The first tree (T_a) begins at the origin q_0 and the second tree (T_b) begins at q_{goal}. After several iterations T_a and T_b are swapped, hence the allocation (T_b,T_a) is not permanent.

The Grasp Region Rapid exploring Random Trees' (GR-RRT) (Reshef, Eizicovits, and Berman 2014) purpose is to incorporate quality of the target configurations into the RRT motion planning algorithm. Thus, allowing more intelligent sampling. The algorithm includes two phases, the offline grasp region determination (GR) and the online planning (Figure 2.6).

The offline GR determination primarily produces graspiblity maps for the required objects. Eventually the configurations are divided into two groups the successful configurations and the not successful configurations this is done using an empirical threshold. The GR is the area encompassing all successful configuration. GR-RRT uses the EM algorithm with BIC criteria to estimate the distributions (Schwarz 1978). The parameters estimated are then delivered to the planner to allow him to sample accordingly.

The online planning phase can now use the offline information (grasp affordance densities) and plan an intelligent path. To insure only successful configurations are selected whenever an out of GR bounds configuration is selected, it is discarded, and new sampling occurs.

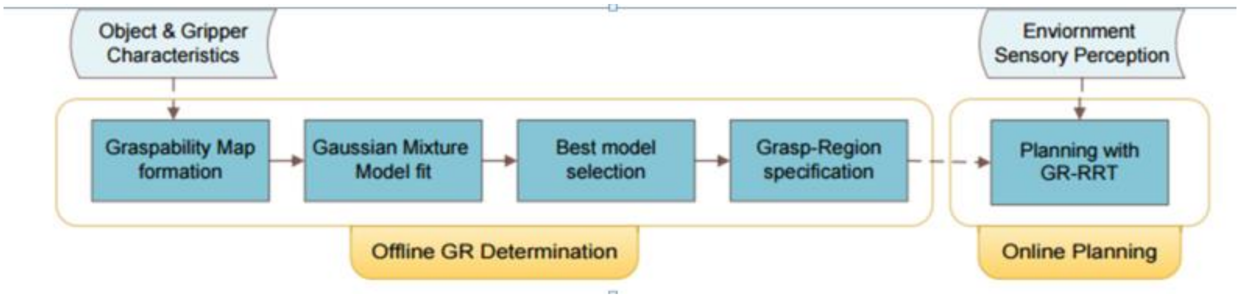

Figure 2.6: GR-RRT algorithm

This algorithm, though slightly more time consuming, produces significantly better results both in path selection and in target configuration selection (Reshef, Eizicovits, and Berman 2014).

2.5. Reach-to-grasp motion of patients with stroke

A stroke can cause temporary or permanent disabilities, depending on how long the brain lacks blood flow and which part was affected. One of the common complications are paralysis or loss of muscle movement. A post stroke patient may become paralyzed on one side of his body, or lose control of certain muscles, such as those on one side of the face or one arm. (Thrasher et al. 2008). Most post stroke patients experience impairment of arm movement, (Lin 2008 , Carr and Shepherd 1998) as a result of the impairment, patients often avoid using the affected arm and compensate the impairment using the other arm or trunk (Michaelsen Dannenbaum, and Levin 2005). The reach to grasp act is often impaired in patients with stroke.

Reaching a specific endpoint arm position can be repeated in different ways. A subject may execute varying movement speeds or one constant speed to different distances (Liebermann et al. 2010). During unimpaired execution of motion, there is a variance in path selection i.e. speed and route, however, after re-executing a similar motion numerous times, movements may follow specific, least effort paths. Patients with stroke demonstrate temporal inefficiency in preplanning and executing movements and rely heavily on feedback control of reaching and grasping (Lin 2008). Liebermann (Liebermann et al. 2010) compared the number of sub movements when reaching to grasp a target in healthy and post stroke subjects, and concluded that post stroke patients showed more sub movements. Lieberman also noticed jerkier movements for patients with stroke.

The orientation adopted by a grasping hand is known to depend on the shape and orientation of the object to be grasped (Desmurget, Prablanc, and Prablanc 1997). In addition, recent studies have demonstrated that it also depends on the spatial characteristics of the task such as the location of the object and initial hand position. It is suggested that not only object location and hand initial position affect variation in hand orientation, but also the movement direction (Bennis and Levin 2003).

Patients with stroke often have weaknesses in distal muscles used to stabilize the wrist, decreased grip strength and lack of fine finger control. These impairments may lead to the development of alternative grasping strategies such as anchoring the fingers on the object to achieve a passive grasp (Roby-Brami et al. 1997).

3. **Non-parametric Bayesian estimation of grasp affordance**

3.1. Overview

In this chapter, the non-parametric Bayesian estimation of grasp affordance algorithm developed is presented in section 3.2. Various tests conducted to examine the limitations and abilities of the algorithm are presented in section 3.3.

3.2. Non- parametric Bayesian estimation algorithm description

The algorithm developed integrates Rasmussen's estimation method, Infinite Gaussian Mixture Model (IGMM) (Rasmussen 2000) and Bangart's VMF estimation method (Bangert 2010). The new combined estimation algorithm (Figure 3.1) is suitable for finding parameters of a combined infinite mixture model, where several degrees of freedom (DOF) are Gaussian and several are VMF. Such a combined mixture model is suitable for representing grasp configurations, in which the three position DOF are modelled using Gaussian distribution components and the three orientation DOF are modelled using VMF distribution components. In Figure 3.1, The bold box indicates an addition to the algorithm and the broken line boxes indicates a stage modification.

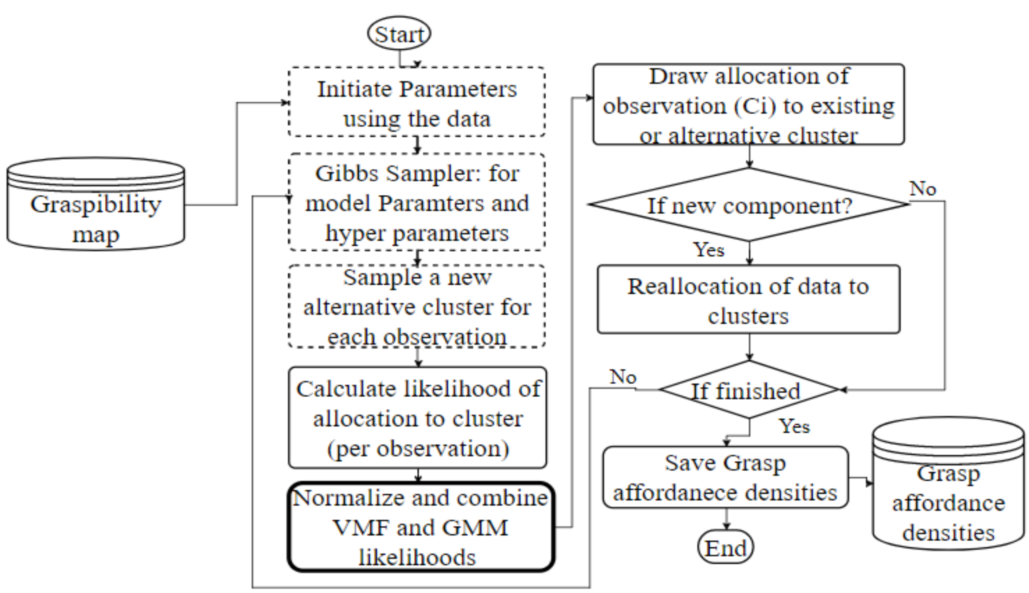

Figure 3.1: Non-parametric Bayesian estimation algorithm – flow chart

The algorithm starts with an initiation stage, an assumption that all data points are allocated to one cluster is made (Rasmussen 2000). The parameters are initiated using maximum likelihood estimators given the original data. The original VMF estimation method set the hyper parameters to constants, we attempted to modify the estimation of the hyper parameters. However due to numeric problems we only changed the hyper parameters (m,t) to be initiated using maximum likelihood estimators, and left the hyper parameters (a,b) constant.

For the Von Misses-Fisher distribution, kappa, the concentration parameter is estimated using: $\widehat{kappa} \approx \frac{\bar{r}d-\bar{r}^3}{1-\bar{r}^2}$ (Banerjee 2005) Where d is the number of dimensions and $r = \sum_i x_i$. The VMF mean parameter (u_{cyc}) is initiated using $\hat{\mu} = \frac{r}{\sqrt{r^2}}$ where $r = \sum_i x_i$. The hyper-parameters for the mean parameter (m,t) are initiated using maximum likelihood, where m (expected direction parameter) is equal to $\hat{\mu}$ and t (concentration parameter) is equal to the initiation of the parameter kappa. For the Gaussian parameters the initiation of the location was done following Rasmussen's work (Rasmussen 2000).

The conjugate prior distributions are presented in table 1. The parameters of a specific cluster i ($\mu_i, \sigma_i, kappa_i, \mu_{cyc_i}$) are estimated using the data observations allocated to the i'th cluster. Differently, the hyper parameters, are estimated using all data observations regardless of the allocation to clusters.

TABLE **1** : Parameters and hyper parameters' distributions

Parameter	Distribution chosen for parameters	Distribution chosen for estimation of hyper - parameters
Infinite GMM		
μ- Mean parameter	Normal (λ, r^{-1}) Where λ is the mean parameter and r is precision parameter	$p(\lambda)$~Normal (μ_y,σ_y^2) where μ_y is the mean of all observations and σ_y^2 is the variance of all observations
		$p(r)$~Gamma $(1,\sigma_y^{-2})$ where σ_y^{-2} is the inverse variance of all observations

S- Precision parameter	Gamma (β,w^{-1}) Where w is the mean parameter and β is shape parameter	$p(w)$~Gamma (1,σ_y^2) where σ_y^2 is the variance of all observations
		$p(\beta)$~Inverse Gamma (1,1)
Infinite VMF		
μ_{cyc}- Mean parameter	Von Misses Fisher (m , t) Where m is the mean parameter and t is concentration parameter	m =Maximum likelihood (μ_{cyc_y}) where μ_{cyc_y} is the cyclic mean of all observations
		t =Maximum likelihood ($kappa_y$) where $kappa_y$ is the concentration parameter of all observations
Kappa-Concentration parameter	$f(\tau_k; a, b) \propto \{\frac{\tau_k}{4\pi \sinh(\tau_k)}\}^a e^{\tau_k b}$ where 'a' and 'b' are scalar parameters a>b>0	a =Constant
		b =Constant
Mixing Parameter		
C-Discrete Indicator	Diriclet ($\frac{\alpha}{k} \dots \frac{\alpha}{k}$) Where k is the number of clusters and α is a scalar	$p(\alpha^{-1})$~Gamma (1,1)

The posterior conditional distributions (equations 14-19) follow Bangart and Rasmussen's work with adaptations (Bangert 2010, Rasmussen 2000). Similarly to the initiation stage, In Bangart's algorithm (Bangert 2010) the hyper parameters of VMF distribution(m, t, a, b) remain constant throughout all estimation iterations. Thus, the same modification explained in initiation was performed for the hyper parameter estimation.

Translation parameters and hyper parameters (Rasmussen 2000)

$$p(\mu_j|\mathrm{c}, \mathrm{y}, s_j, \lambda, r) \sim Normal\left(\frac{\overline{y_j} n_j s_j + \lambda r}{n_j s_j + r}, \frac{1}{n_j s_j + r}\right) \tag{14}$$

$$p(\lambda|\mu_1, \dots, \mu_k, r) \sim Normal\left(\frac{\mu_y\ \sigma_y^{-2} + r \sum_{j=1}^{k} \mu_j}{\sigma_y^{-2} + kr}, \frac{1}{\sigma_y^{-2} + kr}\right) \tag{15}$$

$$p(r|\mu_1, \dots, \mu_k, \lambda) \sim G\mathrm{amma}(k+1, [\frac{1}{k+1}(\sigma_y^2 + \sum_{j=1}^{k}(\mu_j - \lambda)^2]^{-1}) \tag{16}$$

$$p(s_j|\mathrm{c}, \mathrm{y}, u_j, \beta, w) \sim Gamma(\beta + n_j,\ [\frac{1}{\beta + n_j}(\mathrm{w}\beta + \ \sum_{i:c_i=j}\left(y_i - u_j\right)^2)]^{-1}) \tag{17}$$

$$p(w|s_1, \dots, s_k, \beta) \sim Gamma(k\beta + 1, [\frac{1}{k\beta + 1}\left(\sigma_y^{-2} + \beta \sum_{j=1}^{k} s_j\right)]^{-1}) \tag{18}$$

$$\mathrm{p}(\beta|s_1, \dots, s_k, w) \propto \Gamma\left(\frac{\beta}{2}\right)^{-k} \exp\left(\frac{-1}{2\beta}\right)\left(\frac{\beta}{2}\right)^{\frac{k\beta-3}{2}} \Pi\left(s_j w\right)^{\frac{\beta}{2}} \exp\left(-\frac{\beta s_j w}{2}\right) \tag{19}$$

Where y_i represents the three position parameters of data sample 'i', n_j is the number of observations allocated to cluster 'j' and 'k' indicates the number of clusters, the rest of the parameters are presented in table 1. The latter density is not of standard form, but it can be shown that $\mathrm{p}(\beta|s_1, \dots, s_k, w)$ is log-concave, so we may generate independent samples from the distribution for log (β) using Adaptive Rejection Sampling (ARS) technique.

Orientation parameters (Bangert 2010):

$$p(T_j|a, b, \{x_{i\in k}\}, \mu_j) \propto \mathrm{f}(\left\{\frac{T_j}{4\pi\, sinh(T_j)}\right\}^{a+n_j} \exp(T_j * \left(b + \sum_{i\in k} \mu_{cyc}{}_k^T x_i\right)) \tag{20}$$

$$p(\mu_j|\{x_{i\in k}\}, T_j, m_o, t_0) \propto \frac{|m_o t_0 + T_k \sum_{i\in k} x_i|}{4\pi sinh(|m_o t_0 + T_j \sum_{i\in k} x_i|)} \exp(T\left(\frac{m_o t_0 + T_j \sum_{i\in k} x_i}{|m_o t_0 + T_j \sum_{i\in k} x_i|}\right)^T x) \tag{21}$$

Where x_i is the orientation parameters of data sample 'i', the rest of the parameters are presented in table 1. The kappa parameter's posterior conditional distribution is a complex function (equation 20), requiring a suitable sampling method such as slice sampling algorithm (Neal 2003). Still, when encountering a cluster with many observation samples, numeric problems occur. Therefore, when the algorithm encounters a cluster with many observations, the algorithm randomly selects a portion of observations from the cluster.

Mixing parameters:

Components with more than one data sample allocated

Gaussian: $$p(c_i = j|c_{-i}, u_j, s_j, a) \propto p(c_i = j|c_{-i}, a)p(y_i|c_{-i}, u_j, s_j) \tag{22}$$

VMF $$p(c_i = j|c_{-i}, u_j, s_j, a) \propto p(c_i = j|c_{-i}, a)p(x_i|c_{-i}, u_j, kappa_j) \tag{23}$$

All other components combined:

Gaussian $$p(c_i \neq c_{i'}\ for\ all\ i \neq i'|c_{-i}, a) \int p(y_i|u_j, s_j)p(u_j, s_j|\lambda, r, \beta, w)du_j ds_j \tag{24}$$

VMF: $$p(c_i \neq c_{i'}\ for\ all\ i \neq i'|c_{-i}, a) \int p(x_i|u_j, kappa)p(u_j, kappa_j|a, b, t, m)du_j dkappa_j \tag{25}$$

where the subscript '−i ' indicates all indexes except 'i', x_i is the orientation parameters of data sample 'i', y_i is the position parameters of data sample 'i'. The rest of the parameters are presented in table 1. The estimation of the parameters for the translation and orientation (equations 14-21) were done independently. However, determining the observation allocation to a cluster and whether a new cluster arouse, considers both translation and orientation parameters. To combine the Gaussian and VMF probabilities we normalized the probabilities and gave weights to both translation and orientation probabilities. This stage is illustrated in the bold box in Figure 3.1. Once a new cluster is proposed, reallocation of the data occurs, and a new iteration begins. Only clusters which represent more than one sample remain in the following iteration.

3.3. Validation experiment

To validate the algorithm an examination of each, position and orientation, based estimation were tested alone and combined. Data sets with different levels of overlap between clusters were examined to understand the abilities and limitations of the algorithm.

3.2.1. Data

Four different sets of synthetic data were generated, the first set of synthetic data generated was from distinctly different clusters both in orientation and in position. The first data set was used for validation and three types of estimations were carried, estimation by position only, estimation by orientation only and estimation integrating both position and orientation. The second data set, tested the algorithm's performance when an overlap in position existed and a distinct separation in orientation (OP). The third data set tested the algorithm given an overlap in orientation and a distinct separation in position (OO). Lastly, the fourth data set tested the algorithm given an overlap in both position and orientation (OPO).

500 samples were generated from each data set (data set parameters presented in appendix 1) using the random mixture model sampling algorithm specified in section 4.2.1 and then used as input to the non-parametric Bayesian algorithm specified in section 3.2.

3.3.2. Experimental protocol

15000 iterations were performed using the grasp affordance density algorithm, hyper parameters of the VMF concentration parameter, kappa, are constants, and set to a=5, b=4.7 the values were determined following Bangart (Bangert 2010). And the hyper parameter of the Dirichlet distribution is drawn from an inverse gamma distribution G~(1,1). The likelihoods (VMF and Gaussian) determining the allocation of a sample to cluster were given equal weights (0.5,0.5). Sampling kappa using the slice sampling algorithm (VMF concentration parameter) was done based on one hundred randomly selected samples with a burning in value of 5. The final iteration of the algorithm is used as the selected model where clusters which weigh less than 5% are discarded. To compare the goodness of fit visual graphs are generated and examined.

3.3.3. Results

3.3.3.1. Validation Set: Distinct separation of both orientation and position

For estimation by position only, the algorithm converged after about 3500 samples. The affordance densities established, includes three clusters (Figure 3.2-3.3, table 2). The position expected value is 0.57 ± 0.01 cm away from the ground truth. The weights of the cluster are (0.33,0.338,0.332) compared with (0.33,0.33,0.33) and the variance is also very similar (Appendix 1). Though the allocation of data did not consider the orientation components the estimated expected value of the orientation is very close to the ground truth and is only 0.65 ± 0.14 degrees apart. The concentration of the orientation data is lower than the concentration of the ground truth (Appendix 1).

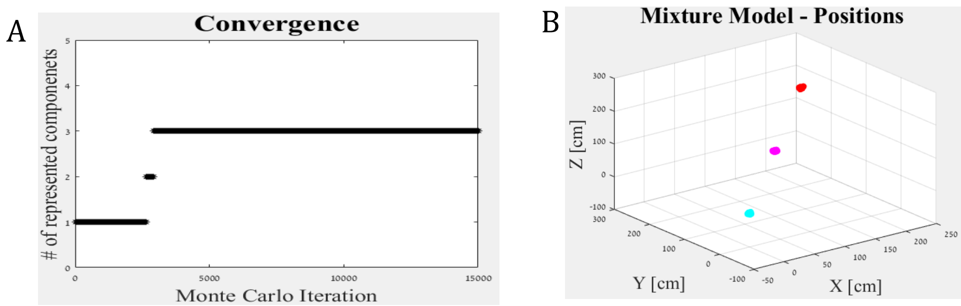

Figure 3.2: Position only- mixture model

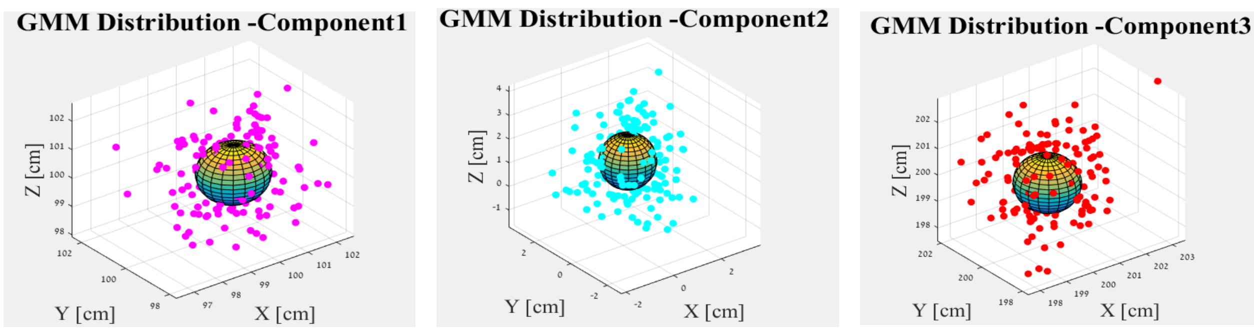

Figure 3.3: Position only - distribution by component

The ellipsoid represents the cluster which the algorithm found fit where the center of the ellipsoid represents The expected value and the circumference is one standard deviation away from the center

TABLE 2: Position only- parameters per cluster

Cluster	1	2	3
Weight	0.33	0.338	0.332
		Position	
μ	[100.03,99.85,100.08]	[0.95,0.98,1.07]	[199.9,199.84,199.94]
S	1.2,-0.02,0.04 -0.02,1.05,0.09 0.04,0.09,0.97	0.95,0.01,0.10 0.01,0.96,0.06 0.1,0.06,1.21	1.05,0.04,0.07 0.04,1.14,0.12 0.07,0.12,1.01
		Orientation	
Kappa	107.88	100.75	94.42
μ_{cyc}	[0,1,-0.01,0]	[0,-0.01,0.71,0.71]	[0.01,0.72,0.7,0]

For estimation by orientation only, the algorithm converged after about 3000 samples. The affordance densities established, includes three clusters (Figure 3.4-3.5, table 3). The orientation expected value is 0.81 ± 0.41 degrees away from the ground truth, the weights of the cluster are (0.33,0.338,0.332) compared with (0.33,0.33,0.33) and the concentration of the orientation data is lower than the concentration of the ground truth (Appendix 1). Though the allocation of data did not consider the position components the position expected value is very close to the ground truth and is only 0.21 ± 0.13 cm apart. and the variance is also very similar (Appendix 1).

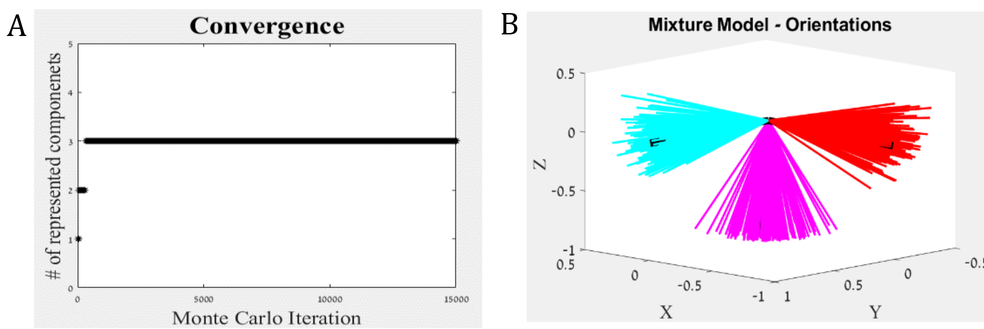

Figure 3.4: Orientation only- mixture model and convergence
The black lines represent the direction (expected value) of the cluster

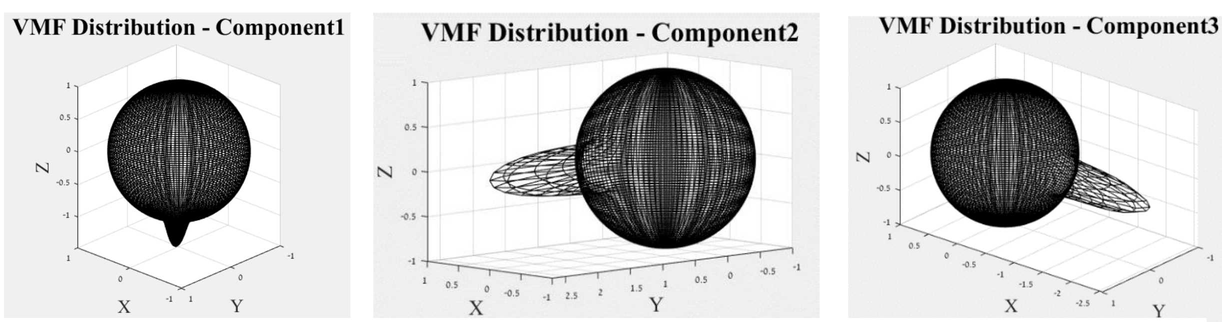

Figure 3.5: Orientation only - distribution by component

TABLE 3: Orientation only-parameters per component

Cluster	1	2	3
Weight	0.338	0.33	0.332
Position			
μ	[0.88,0.87,1.11]	[99.96,99.98,100.08]	[200.04,199.99,200.07]
S	1.06,0.19,0.02 0.19,0.93,-0.03	1.08,0.09,0.03 0.09,0.84,0.09	0.89,0.02,0.16 0.02,1.01,0

	0.02,-0.03,1.47	0.03,0.09,1.3	0.16,0,1.17
Orientation			
Kappa	118.39	74.09	81.11
μ_{cyc}	[-0.01,0, 0.7,0.71]	[0,1, 0.01,0.01]	[-0.01,0.71,0.7, 0.02]

Estimation given both position and orientation integrated, the algorithm converged after about 200 iterations. The affordance densities established, includes three clusters (Figure 3.6-3.7, table 4). The position expected value is 0.27 ± 0.09 cm away from the ground truth, the weights of the cluster are (0.33,0.338,0.332) compared with (0.33,0.33,0.33) and the variance is also very similar (Appendix 1). The orientation expected value is very close to the ground truth and is only 0.89 ± 0.24 degrees apart. The concentration of the orientation data is lower than the concentration of the ground truth (Appendix 1).

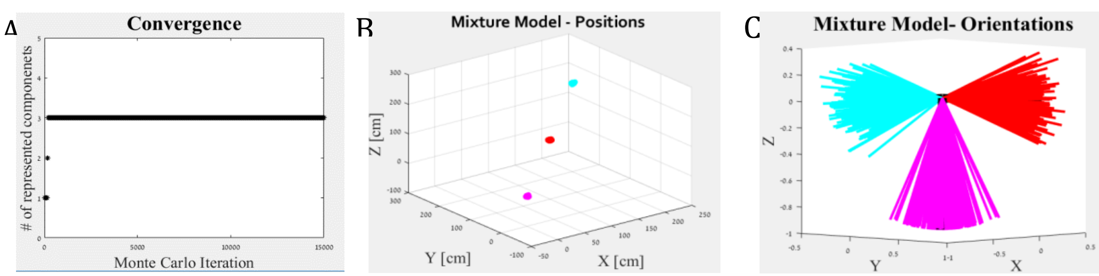

Figure 3.6: integrated algorithm- Convergence and mixture model

Quaternions and positions are colored according to the cluster they are allocated to. The black lines in figure C represent the direction (expected value) of the cluster.

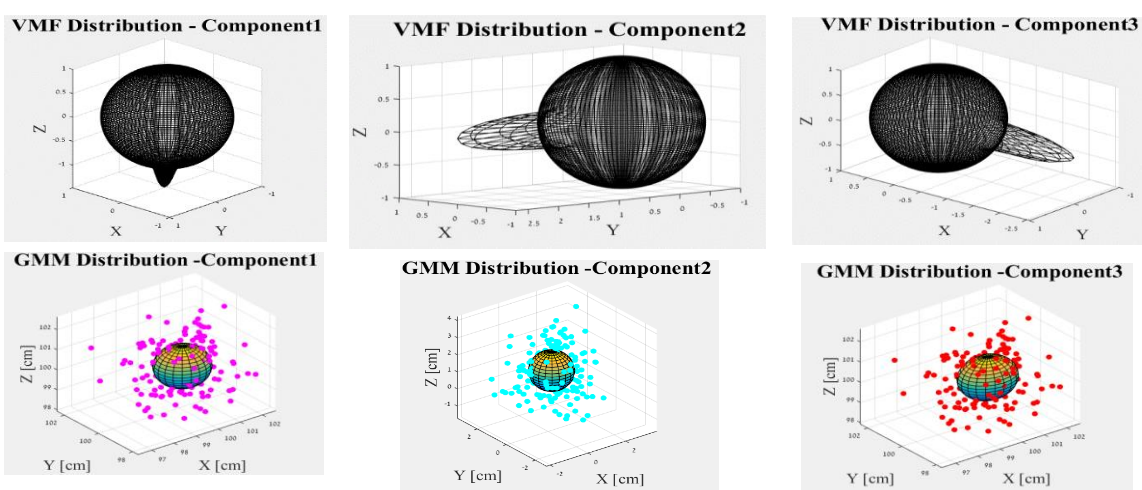

Figure 3.7: Integrated algorithm- distribution by component

The ellipsoid represents the cluster which the algorithm found fit where the center of the ellipsoid represents the expected value and the circumference is one standard deviation away from the center

Cluster	1	2	. 3
Weight	0.338	0.332	0.33
Position			
μ	[0.94,0.95,1.12]	[200.07,199.89,200.2]	[100.21,100, 100]
S	1.17,0.13,0.07 0.13,1.08,0.09 0.07,0.09,1.21	1.17,.16,0.19 0.16,1.09,0.23 0.19,0.23,1.32	1.4,0.12,0.05 0.12,0.92,-0.01 0.05,-0.01,1.03
Orientation			
Kappa	98.75	108.3	101.56
μ_{cyc}	[0.005,-0.013,0.718,0.696]	[-0.006,0.716,0.698,-0.007]	[-0.001,1,-0.01, 0.007]

TABLE 4: Integrated algorithm - parameters per component

3.3.3.2. Overlap Position dataset (OP): Distinct separation of orientation and overlap in position

The samples generated are demonstrated in Figure 3.8, the model parameters used to generate the samples are presented in Appendix 1.

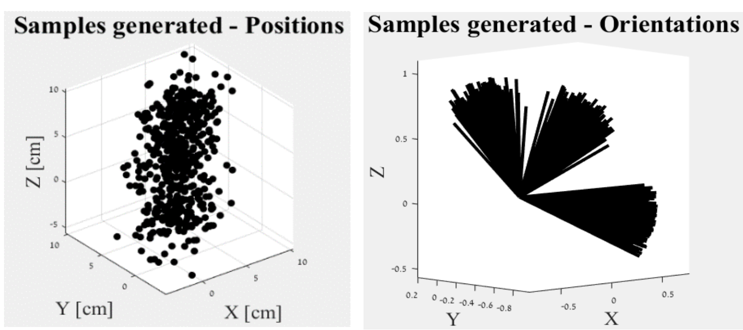

Figure 3.8: Position overlap - samples generated

Estimation given both position and orientation integrated, the algorithm converged after about 300 iterations. The affordance densities established, includes three clusters (Figure 3.9-3.10, table 5). The position expected value is 0.66 ± 0.23 cm away from the ground truth, the weights of the cluster are (0.322,0.39,0.288) compared with (0.33,0.33,0.33) and the variance is also very similar (Appendix 1). The orientation estimated expected value is very close to the ground truth and is only 3.24 ± 1.9 degrees apart. The concentration of the orientation data is lower than the concentration of the ground truth (Appendix 1).

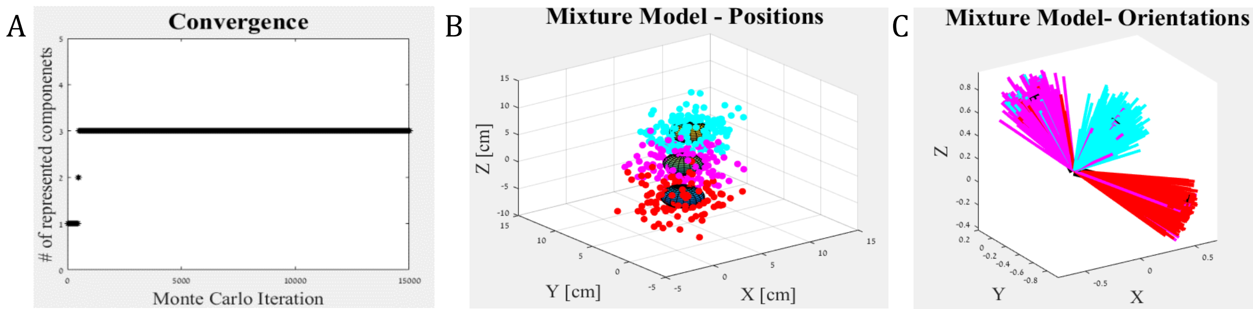

Figure 3.9: Translation overlap- convergence and mixture model-

Quaternions and positions are colored according to the cluster they are allocated to. The black lines in figure C represent the direction (expected value) of the cluster.

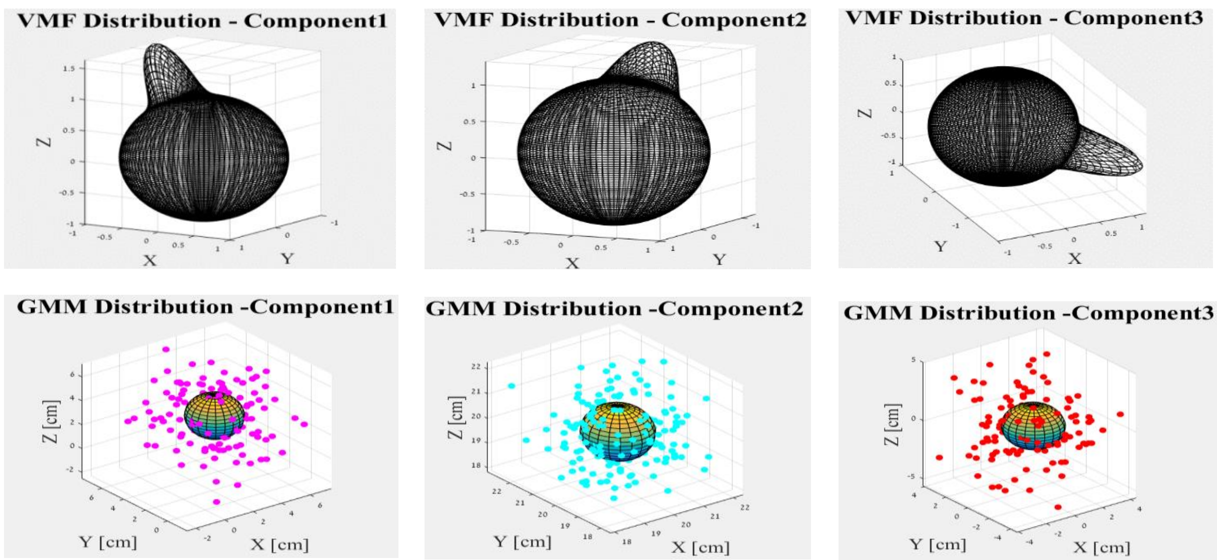

Figure 3.10: Translation overlap – distribution by component

The ellipsoid represents the cluster which the algorithm found fit where the center of the ellipsoid represents. The expected value and the circumference is one standard deviation away from the center

TABLE 5: Position overlap -parameters per component

Cluster	1	2	3
Weight	0.322	0.39	0.288
Position			
μ	[2.67,3.25,3.11]	[6.24,5.85,6.03]	[-0.16,-0.42,-0.3]
S	3.73,0.1,0.12 0.1,3.11, 0.13 0.17,0.13,2.99	2.78,-0.01,0.39 -0.01,2.57,0.12 0.39,0.12,2.6	2.95,-0.32,0.06 -0.32,2.97,0.39 0.06,0.39,4.18
Orientation			
Kappa	45.2	42.16	49.74
μ_{cyc}	[0.737,0.474,-0.235,0.4190]	[0.86,0.361,0.34,-0.12]	[0.469,0.195,-0.845,-0.169]

3.3.3.3. Overlap Orientation dataset (OO): Distinct separation of position and overlap in orientation

The samples generated are demonstrated in Figure 3.11 the model parameters used to generate the samples are presented in Appendix 1.

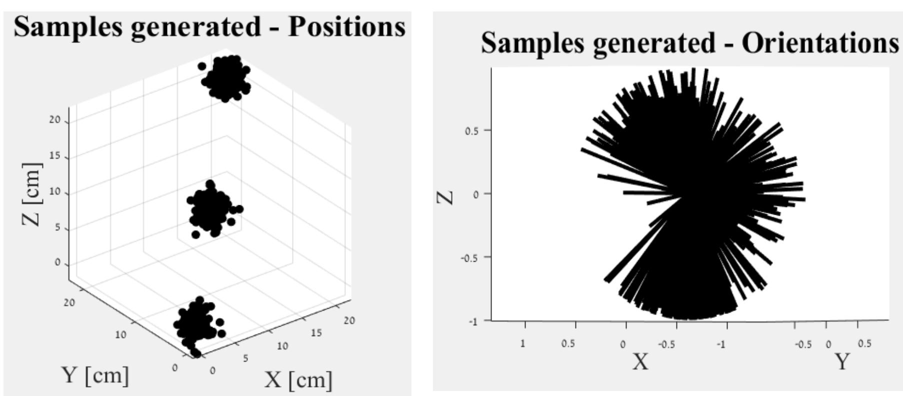

Figure 3.11 Orientation overlap- samples generated

The algorithm converged after 300 iterations. The affordance densities established, includes three clusters (Figure 3.12-3.13, table 6). The position expected value is 0.19 ± 0.04 cm away from the ground truth, the weights of the cluster are (0.348,0.364,0.288) compared with (0.33,0.33,0.33) and the variance is also very similar (Appendix 1). The orientation estimated expected value is very close to the ground truth and is only 2.62 ± 1.88 degrees apart. The concentration of the orientation data is lower than the concentration of the ground truth (Appendix 1).

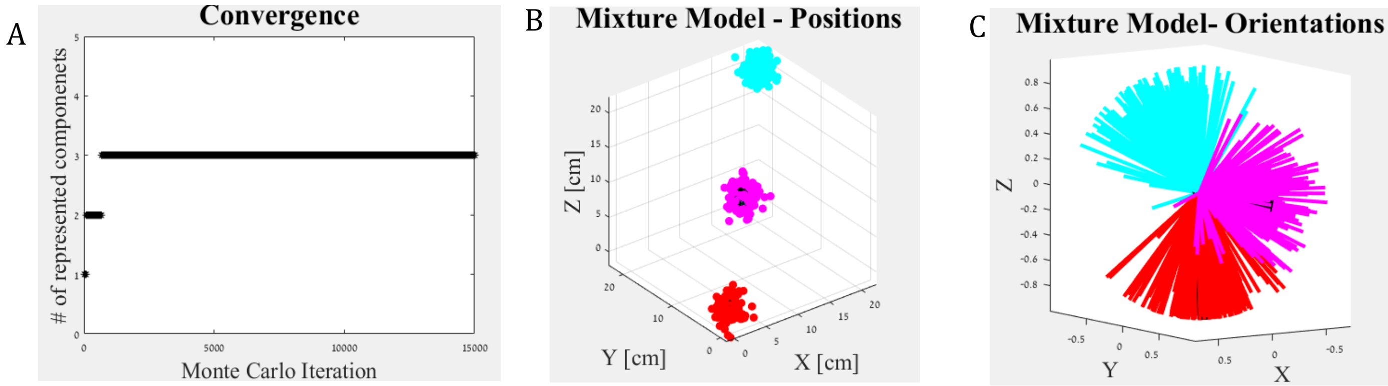

Figure 3.12: Orientation overlap – convergence and mixture model
quaternions and positions are colored according to the cluster they are allocated to. The black lines in figure C represent the direction (expected value) of the cluster.

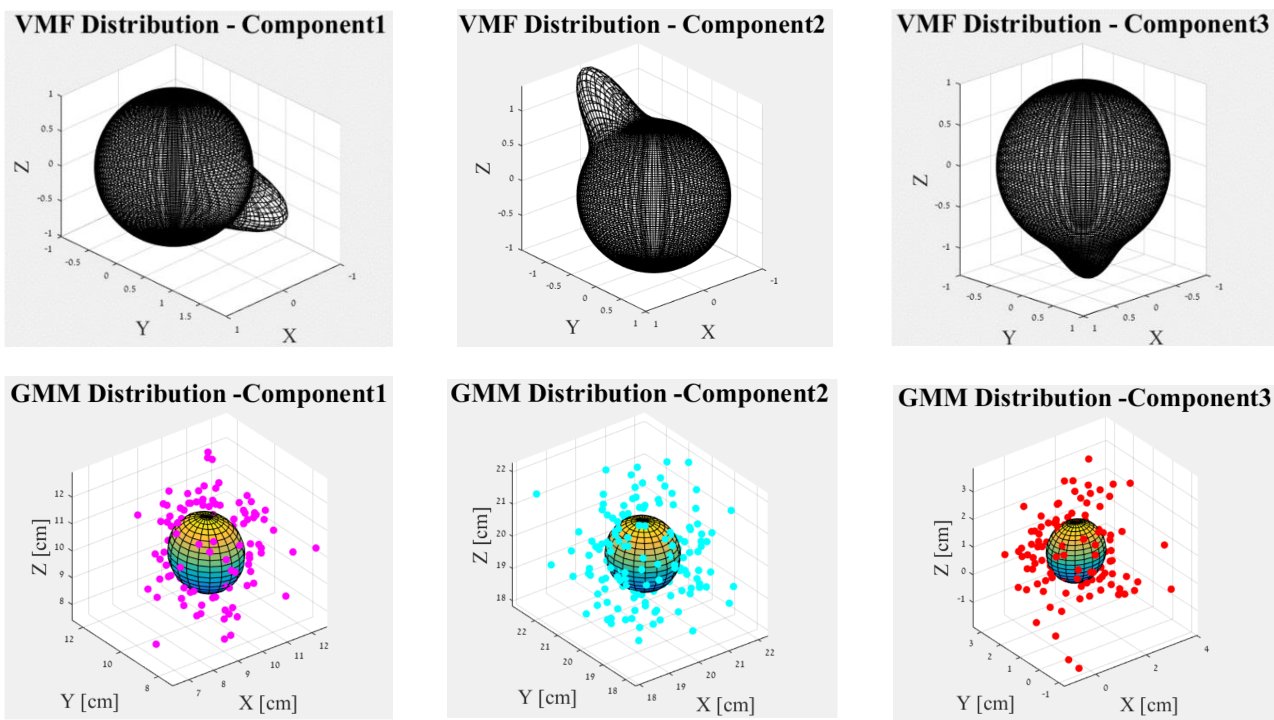

Figure 3.13 Orientation overlap - distribution by component
The ellipsoid represents the cluster which the algorithm found fit where the center of the ellipsoid represents.
The expected value and the circumference is one standard deviation away from the center

TABLE 6: Orientation overlap- parameters per component

Cluster	1	2	3
Weight	0.348	0.364	0.288
Position			
μ	[10.06,10.09,10.07]	[20.05,19.9,20.06]	[1.02,1.04,1.08]
S	1.03,0.25,0.15 0.25,1.16,0.21 0.15,0.21,1.32	1.27,0.08,0.12 0.08,0.95,0.21 0.12,0.21,1.21	1.53,0.48,0.57 0.48,1.29,0.56 0.57,0.56,1.44
Orientation			
Kappa	31.25	30.09	28.43
μ_{cyc}	[-0.036,-0.999,0.007,0.0170]	[0.838,0.342,-0.383,0.185]	[0.687,-0.726,-0.024,0.012]

3.3.3.4. Overlap in Position and Orientation dataset (OTR)

The samples generated are demonstrated in Figure 3.14 the model parameters used to generate the samples are presented in Appendix 1.

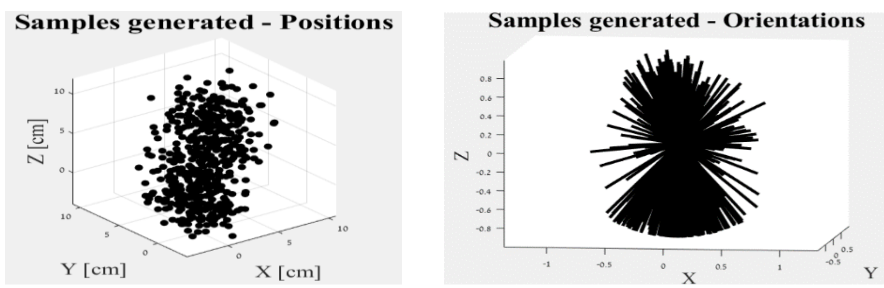

Figure 3.14: Total overlap - samples generated

The algorithm converged after about 300 iterations (Figure 3.15A) however the convergence was not distinct, and the algorithm's number of clusters varied between 2-3 clusters. The affordance densities established, includes three clusters (Figure 3.15-3.16, table 7). The position expected value is 2.62 ± 2.36 cm away from the ground truth, the weights of the cluster are (0.41,0.13,0.46) compared with (0.33,0.33,0.33) and the variance is also very similar (Appendix 1). The orientation estimated expected value (of clusters 1,3) is very close to the ground truth and is only 2.08 ± 0.97 degrees apart and for cluster two, 78 degrees apart. The concentration of the orientation data is lower than the concentration of the ground truth (Appendix 1)

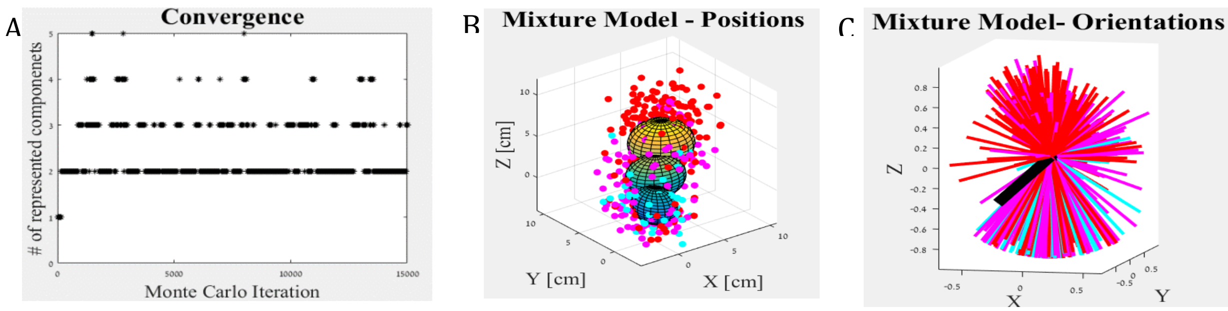

Figure 3.15: Total overlap-convergence and mixture model-

Quaternions and positions are colored according to the cluster they are allocated to. The black lines in figure C represent the direction (expected value) of the cluster. The ellipsoids in figure B represents the cluster which the algorithm found fit, where the center of the ellipsoid represents The expected value and the circumference is one standard deviation away from the center.

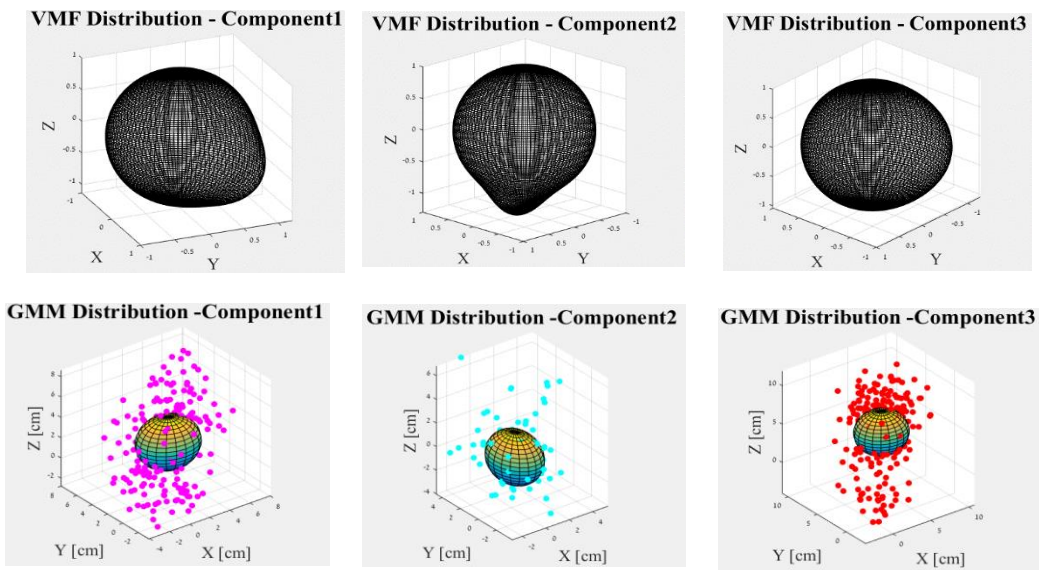

Figure 3.16: Total overlap- distribution by component

The ellipsoid represents the cluster which the algorithm found fit where the center of the ellipsoid represents the expected value and the circumference is one standard deviation away from the center.

TABLE 7: Total overlap- parameters per component

<table>
<tr><td colspan="2">Cluster</td><td>1</td><td>2</td><td>3</td></tr>
<tr><td colspan="2">Weight</td><td>0.41</td><td>0.126</td><td>0.464</td></tr>
<tr><td colspan="5">Position</td></tr>
<tr><td>μ</td><td>[2.2,2.3,1.95]</td><td colspan="2">[0.22,-0.06,0.18]</td><td>[4.3,4.26,4.26]</td></tr>
<tr><td>S</td><td>6.4,2.75,3.12
2.75,5.72,2.69
3.12,2.69,6.1</td><td colspan="2">6.18,0.82,2.75
0.82,5.22,0.56
2.75,0.56,4.2</td><td>8.17, 4.05,4.68
4.05,6.98,4.71
4.68,4.71,8.47</td></tr>
<tr><td colspan="5">Orientation</td></tr>
<tr><td>Kappa</td><td>6.47</td><td colspan="2">15.3</td><td>3.44</td></tr>
<tr><td>μ_{cyc}</td><td>[0.353,-0.935,-0.026, -0.0220]</td><td colspan="2">[0.658,-0.751,-0.026,-0.037]</td><td>[0.939,-0.198,-0.275,0.061]</td></tr>
</table>

3.3.4. Discussion

The estimated models resemble the ground truth but with higher dispersion in the orientation components (kappa). A relatively small overlap between clusters in orientation parameters, significantly impacts the algorithm's ability to distinct between clusters and estimate its true values. A plausible explanation is that the variance in position does not correspond to the variance in orientation. The space characteristics are different for these two distributions, a Gaussian distribution parameter is defined between [-∞,∞] and a VMF parameter distribution is defined between [-180,180].

As for the convergence, it occurs very early i.e. before iteration 1000 in all cases. Thus, even though Rasmussen (Rasmussen 2000) suggested to use 30000 iterations we decided to use 15000 iterations. Furthermore, to avoid a large amount of small, unstable clusters, clusters with a weight of 5% and less are discarded. In table 8 the parameters chosen to initiate the algorithm in the following applications, robotic reach to grasp motion planning and analysis of reach to grasp motion of patients with stroke, are presented.

TABLE 8: Parameter initiation

Parameter	Value
Number of iterations	15000
a- Hyper parameter VMF	5
b- Hyper parameter VMF	4.7
α- Hyper parameter Dirichlet	$G^{-1} \sim (1,1)$
VMF likelihood weight	0.5
GMM likelihood weight	0.5
Slice sampling burning in value	5
Number of randomly selected observations for slice sampling	100

4. **Robotic reach-to-grasp motion planning**

4.1. Overview

The grasps affordance densities used in the GR-RRT algorithm, were modeled by a six-dimensional Gaussian mixture model, and were found separately for each region using EM (Reshef, Eizicovits, and Berman 2014). The division of data between the regions, along with the use of a non-cyclic distribution for estimation of orientation led to models with a high number of components. This complicated the sampling stage during path planning and led to poor generalization. We replaced these models with densities functions modeled using Gaussian functions for positions and VMF functions for orientation, and applied non-parametric Bayesian estimation for model parameter estimation as illustrated in chapter 3. This new method is termed grasp affordance-RRT (GA-RRT). The rest of this chapter is organized as follows: section 4.2 describes the GA-RRT algorithm including the mixture model random sampling algorithm developed. Section 4.3 describes an experiment for testing the GA-RRT algorithm. Results are presented in section 4.4 and a discussion is presented in section 4.5

4.2. GA-RRT algorithm

Like the GR-RRT algorithm the GA-RRT algorithm has two phases, a-priori offline estimation phase (Figure 3.1) and a run-time planning phase (Figure 4.1). The grasp affordance density is derived using non-parametric Bayesian estimation based on graspability maps in the offline estimation phase. During the run-time planning phase, a collision-free path is found using the bi-directional RRT algorithm, where goal configurations are sampled from the grasp affordance density.

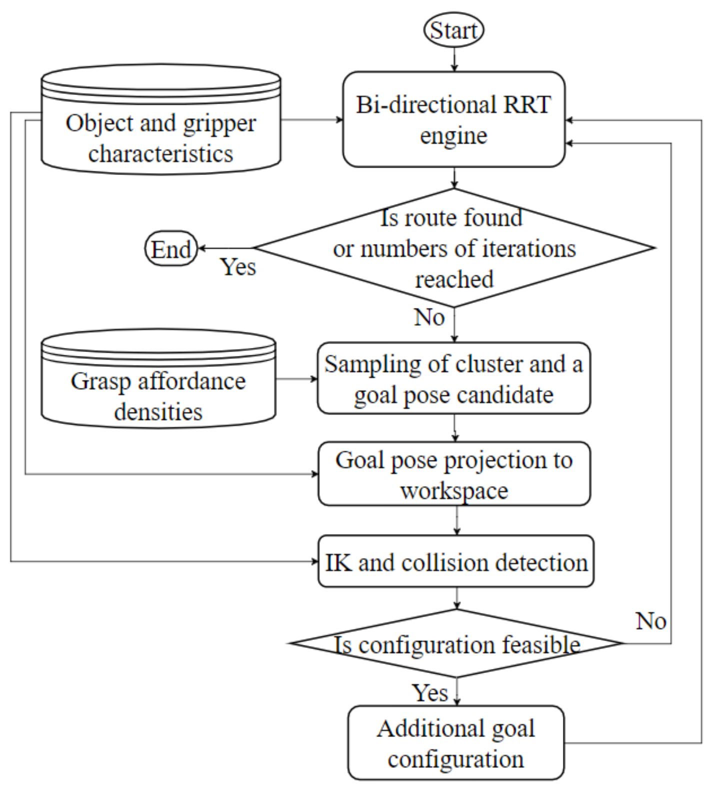

Figure 4.1: Run time planning phase flow chart

The sampling algorithm has two stages (pseudo code below). First, a cluster is sampled with selection probability based on its weight. Second, a configuration is sampled from the selected cluster, where the location and orientation are sampled separately. The location is sampled from the GMM using mvnrnd, the built-in function for sampling GMMs in Matlab™. The orientation is sampled from the VMF mixture model using the random Mises-Fiser sampling algorithm (Jung 2009). To ensure only high quality grasp configurations are used, samples which are far from the mean for both orientation and position are discarded and sampling is re-iterated. For the position, samples within 3σ range are kept. Orientation is represented by a quaternion (q_0, q_1, q_2, q_3). The distance from the mean is evaluated separately for the direction vector and for rotation angle (q_0). Only samples where both are within $\frac{1}{3*kappa}$ range are kept.

Algorithm random configuration sampling

$[\mu_i, \sigma_i, kappa_i, \mu_{cyc_i}]$ = getClusterDist ()

The function getClusterDist (), draws a cluster ID, randomly according to cluster weight and sets the parameter values according to the parameters of the selected cluster

Do [xyz]= mvnrnd(μ_i, σ_i)
While($\mu_i - 3\sigma_i > xyz$ ***or*** $\mu_i + 3\sigma_i < xyz$)

Do[quaternion]=vmfrnd($kappa_i, \mu_{cyc_i}$)

$$\theta = \arccos\left(\frac{\overrightarrow{\mu_{cyc_i}} * \overrightarrow{\text{quaternion}[1:3]}}{\left\|\overrightarrow{\mu_{cyc_i}}\right\| * \left\|\overrightarrow{\text{quaternion}[1:3]}\right\|}\right.$$

While ($\frac{-1}{3*kappa} > \theta$ ***or*** $\frac{1}{3*kappa} < \theta$ ***or***
$\frac{-1}{3*kappa} >$ quaternion[0] ***or*** $\frac{1}{3*kappa} <$ quaternion[0])

Return sample=[xyz,quaternion]

4.3. Experiment

4.3.1. Object and Environment

A mug with multiple grasping regions and a jaw gripper were modeled in simulation (Figure 4.2-4.3). The simulated environment was modeled based on the Telerobotics lab, the Industrial Engineering Dept. at the Ben-Gurion University (Figure 4.4). It comprised a six DOF manipulator (UP6, MOTOMAN, Japan) with a two-jaw gripper (HGPL-25-60-A, FESTO, Germany), a table placed within the robot's reach, and wooden blocks that served as obstacles. Five compositions of the blocks and the object location were created for each object (Figure 4.5). (Eizicovits and Berman 2014). A graspibility map containing 1500 grasps was generated for the gripper and mug by a robotic expert, (Figure 4.6). The grasps included three general types of grasps, one grasping the mug handle, and two grasps types grasping the mug body. The estimation algorithm and simulation were executed with MATLAB (Version 2016A, Mathworks, USA) using an Intel® i7-5500U, 2.4GHz CPU, with 8GB 2.4GHz RAM running Windows 10.

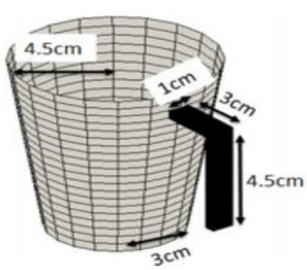

Figure 4.2: Mug's dimensions

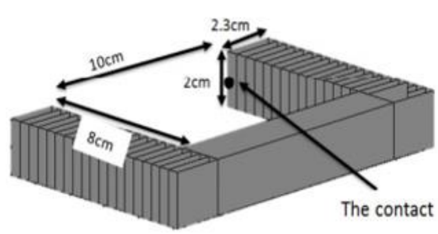

Figure 4.3: Grippers dimensions

Figure 4.4: The physical environment in the telerobotic laboratory

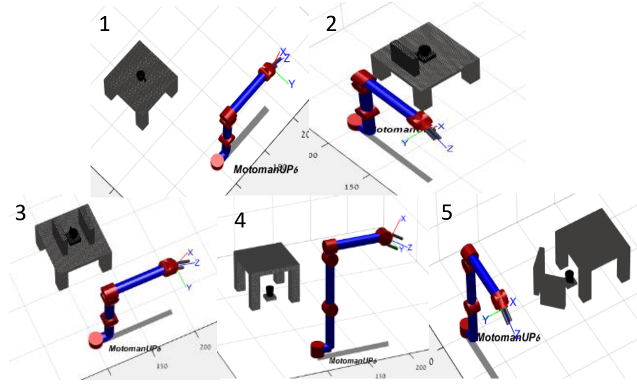

Figure 4.5: The five environment compositions. In all compositions, the mug was placed each one of the environments.

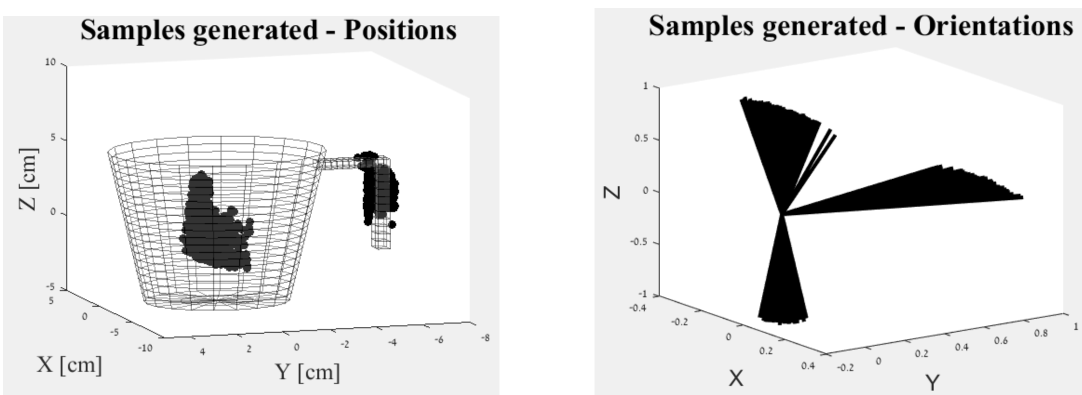

Figure 4.6: Grasp configurations generated by expert

4.3.2. Experimental protocol

Distribution estimation parameters were initiated according to table 8. The probability of choosing to add a configuration over expanding the RRT tree, P_{sample}, was set to 0.15. Planning was executed 20 times per environment composition (compositions one to five). The maximum number of iterations was set to 20,000. Each resulting path was smoothed using a path smoothing method based on vertices removal (Reshef and Berman 2013). The configuration used for analysis is the Tool Centre Point (TCP).

4.3.3. Analysis

Algorithm performance was evaluated in terms of computation time, path quality, and grasp success. Path quality was quantified by the final path length in the configuration space, using two normalized distance measures: Euclidean distance, ND_e (equation 26) and City-block distance, ND_{cb} (equation 27).

$$ND_e = \frac{\sum_{i=2}^{V}\sqrt{\sum_{j=1}^{J}(x_{i,j}-x_{i-1,j})^2}}{\sqrt{\sum_{j=1}^{J}(x_{i,j}-x_{V,j})^2}} - 1 \tag{26}$$

Where $x_{i,j}$ (in deg) is the position of the i^{th} vertex in the j^{th} dimension of the configuration space, V is the total number of vertices in the path, and J is the total number of manipulator joints (six in our experiment).

$$NDcb = \frac{\sum_{i=2}^{V}\sum_{j=1}^{J}|x_{i,j}-x_{i-1,j}|}{\sum_{j=1}^{J}|x_{i,j}-x_{V,j}|} - 1 \tag{27}$$

Both measures are normalized to start at zero, for the shortest possible path. The Euclidean distance, ND_e, reflects the distance with respect to the minimal movement length and thus is related to shortest mission execution time. While the City-block distance, ND_{cb}, reflects distance with respect to minimal movement of each joint, and thus is related to a minimal motor effort.

A considerable number of paths were along the line-of-sight to the target pose (both ND_e and ND_{cb} are 0), thus the analysis of path quality was divided into two categories. Grasps where the Euclidean distance was equal to the line-of-sight and others.

Grasp success was evaluated by projecting the sampled pose back onto the graspability map. The grasp was determined as successful (‘1’) in case of a grasp of quality grade of 0.7 or above, and as unsuccessful (‘0’) otherwise.

4.4. Results

The algorithm converged very fast after about 100 samples. The affordance densities established, includes three clusters (Figure 4.7-4.8, table 9). The estimated model represents the data comprehensively and demonstrates the three grasp types which were expected.

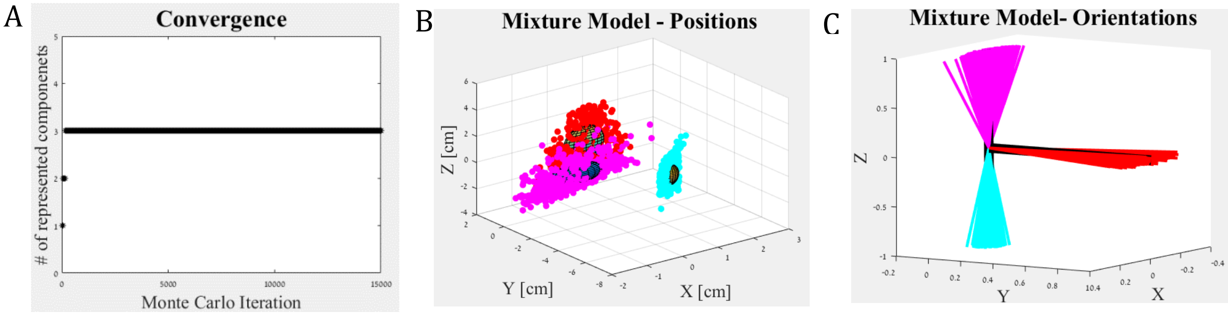

Figure 4.7: Mug convergence and mixture model

Data points and quaternions are colored according to the cluster they are allocated to. The center of the ellipsoid represents the mean and the circumference is one standard deviation away from the center.

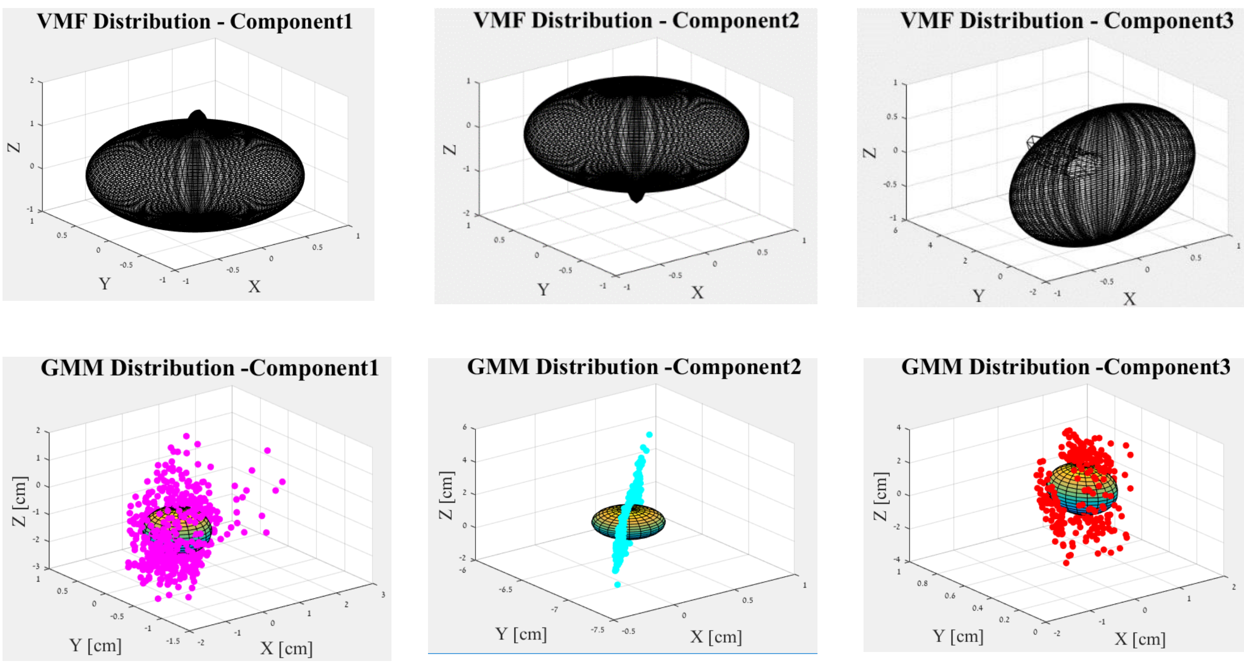

Figure 4.8: Mug distribution by component

TABLE 9: Mug-Parameters per component

Cluster	1	2	3
Weight	0.44	0.31	0.25
Position			
μ	[0.07, 0.07, -1.45]	[0.02,-6.98,1.74]	[0.48,0.54,0.36]
S	0.54,0.18,0.09 0.18,0.15,0.01 0.09,0.01,0.65	0.06,0.06,0.03 0.06,0.06,0.03 0.03,0.03,0.62	0.33,0.07,0.11 0.07,0.03,0.02 0.11,0.02,1.96

Orientation			
Kappa	235	336	276.8
μ_{cyc}	[-0.004, 0.005,-0.71,0.704]	[0.707,-0.708,0,0]	[-0.002,-1,-0.002, 0.006]

For environment 5, the algorithm did not find a target point on the mug. In the remainder of the results we will refer to the environments which found at least one target point either successful or not (environments 1,2,3,4).

Average planning time was 4.97±4.6 seconds (Table 10). Path quality: out of the generated paths, 50% were along the line-of-sight to the target pose. In environment composition one (no obstacles) and three (an obstacle in front of the object) all paths were along the line-of-sight. The average values for both distance measures, ND_e and ND_{bc}, were 0.665 and 0.666 respectively (Table 10), which means that for both distance measures the average path required 66%-67% more effort to execute than the lower bound. For grasp success, the average grasp success rate was 95% (Table 10). Examples of grasps per environment are shown in Figures 4.9-4.12.

TABLE 10: Average results per environment

Environment	Euclidean distance, ND_e	City-block distance, ND_{cb}	Time (seconds)	grasp quality grade	Grasp success*
1	0	0	2.38	0.720	95
2	0	0	1.6	0.723	90
3	0.619	0.650	7.21	0.732	95
4	0.711	0.682	8.66	0.809	100
5					
Not line-of-sight path average	0.665	0.666			

*Grasp success calculated assuming quality cutoff for successful grasps.

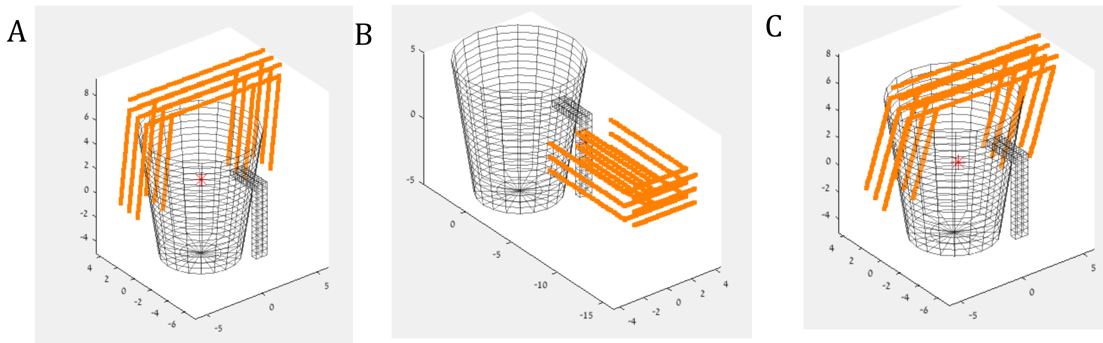

Figure 4.9: Environment 1- representative grasps- the grasp grades are: A =0.77, B=0.88, C=0.75

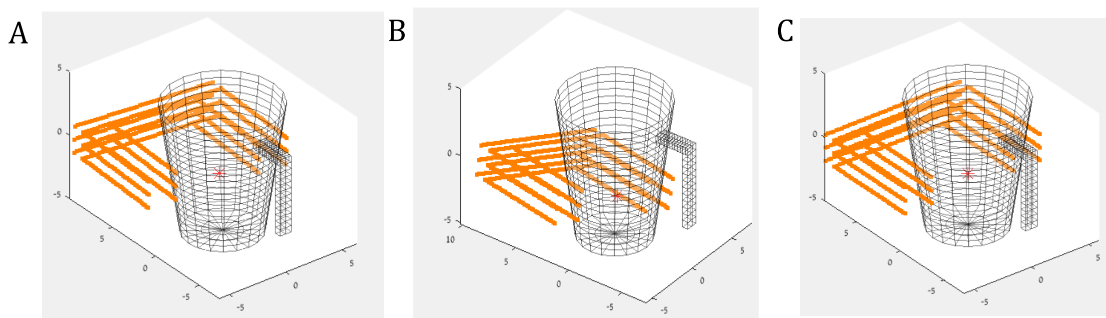

Figure 4.10: Environment 2- representative grasps- the grasp grades are: A =0.76, B=0.61, C=0.75

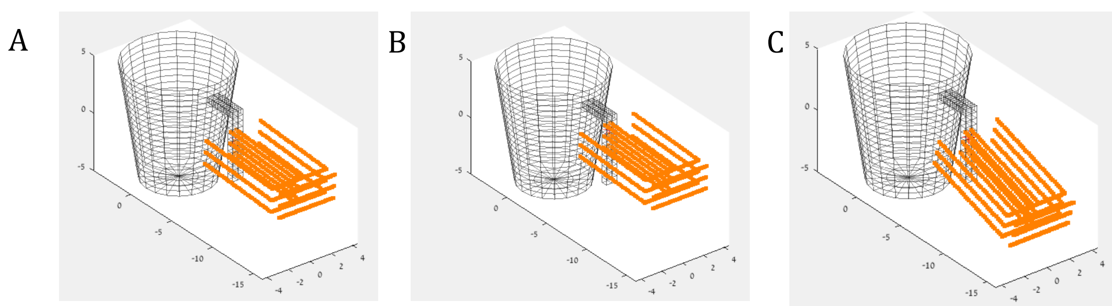

Figure 4.11 Environment 3- representative grasps- the grasp grades are: A =0.81, B=0.79, C=0.80

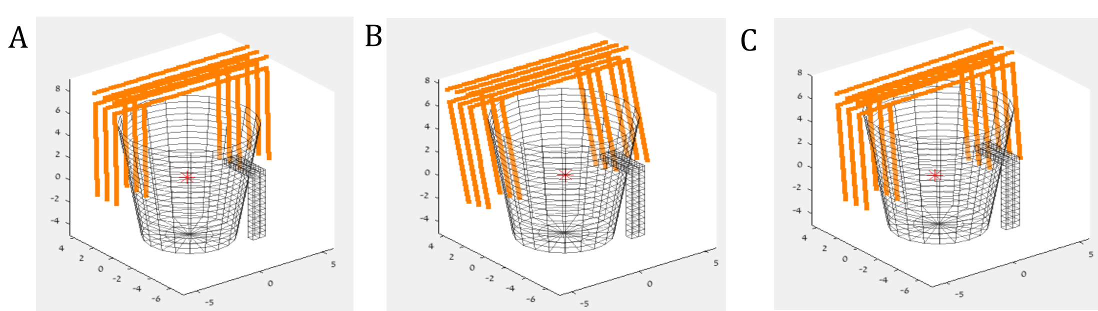

Figure 4.12: Environment 4- representative grasps- the grasp grades are: A =0.77, B=0.76, C=0.75

4.5. Discussion

The estimated model converged fast (after less than 100 iterations), and represents the data comprehensively. Furthermore, the integration introduced by the sampling algorithm performed as expected, and produced configurations that grasped the mug successfully. For one environments, no feasible target poses were found by the algorithm, as all grasps were discarded, due to obstacles, in the path planning stage. This one environment, was very cluttered and required approach orientations that were not included in the original data-base from which the density was estimated. Having a richer graspibility map could help the algorithm in such environments. While in some cases manually defining grasp pose regions may be feasible (Berenson et al. 2009), it is not necessarily representative of the complete distribution of poses that afford high quality grasps. For the environments which a grasp was obtained, the GA-RRT demonstrates a high grasp success rate (95%).

The current work presented an alternative Bayesian based estimation path planning algorithm. Future work should test the GA-RRT algorithm with a richer graspibility map based on additional demonstrations.

5. **Analysis of reach-to-grasp motion of patients with stroke**

5.1. Overview

The study was part of the ENHANCE project (Enhancing brain plasticity for sensorimotor recovery in spastic hemiparesis). The ENHANCE project aims to test the effectiveness of a personalized rehabilitation training program on recovery of voluntary motion of patients with stroke. The training program is based on combination of, motion adaptation to patient capabilities, brain stimulation, and virtual reality. Patient progress is monitored based on clinical and kinematic measurements. The kinematic measurements are based on reach-to-grasp movements performed towards four targets. The current work analyzes wrist configurations at the end of the reach-to-grasp motion. Motion data of patients with stroke was collected prior to the rehabilitation training and after the training (in post training and follow-up sessions). The current work is based only on data recorded before the training, as the post and follow-up trials are sealed until the end of the project. Motion of healthy, control subjects were recorded to from a baseline for comparison. The rest of this chapter is organized as follows: section 5.2 describes the experiment. Results are presented in section 5.3 and discussed in section 5.4.

5.2. Method

5.2.1. Subjects

Participants included 15 subjects with stroke at the subacute stage, 0 to 6 months post stroke of which 6 are left handed (9 males, age 57.4±11 years). And 13 healthy age-matched controls, all right handed (9 males, age 60.46±8.68 years), with no other neurological, sensorimotor, or orthopedic impairments. Subjects with stroke were included in the experiment if they have a first ever stroke in the middle cerebral artery area territory, aged 25-75 years, in the sub-acute stage of the stroke (three weeks to six months post stroke), have arm paresis, able to perform voluntary elbow flexion extension movement of at least 30 degrees, have elbow spasticity and are able to provide informed consent. Subjects were excluded due to clinical issues such as orthopedic problem or pain, major cognitive deficits, history of psychiatric disorders or under medicine treatment. Demographic data of the subjects is presented in Appendix 2.

5.2.2. Environment

Subjects sat on a chair with feet supported and their hand resting alongside body (elbow extended to 180 degrees). The chair had a back support that did not restrict trunk movements. Four targets (standard hollow cones about 10 mm radius × 30 mm height) were placed on the table in front of the subject (Figure 5.1). Two target locations were in the mid-sagittal plane, one at 2/3rd of arm's length (Target 1 – Near Center target (NC)) and one at arm's length (Target 2 – Far Center target(FC)). Target 3 - Far Left (FL) and Target 4 - Far Right target (FR) targets were placed at arm's length, about 20-30 cm to the left, depending on and within reaching distance, respectively (Figure 5.2).

Movements were recorded with a wireless electromagnetic tracking system G4™ Polhemus (Figure 5.3). The reported root mean square static accuracy of this system is 0.08 inches for position and 0.50 degrees for orientation when used within 1 meter of the source. Each sensor has 6 degrees-of-freedom and is tracked at 120Hz. Five sensors (denoted M1-M5) were used to track the position of the upper limb, shoulder girdle, and trunk in real-time. Sensors were placed on the metacarpi-phalangeal (MCP) joint of the index finger (M1), on the dorsal surface of the forearm (1/3 of the length of the forearm proximal to the head of the ulna), on the lateral surface of the upper arm at about the middle of the upper-arm (M3), on the mid-point of the superior-lateral border of the acromion (M4), and on the mid-sternum (M5). All experiment recordings were saved as MicrosoftExcel™ files using Matlab™.

Figure 5.1: Cones for grasp

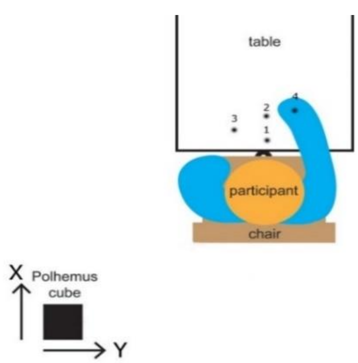

Figure 5.2 : Experimental setup

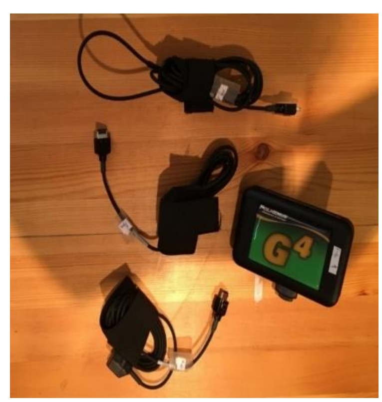

Figure 5.3 : G4 tracking system

5.2.3. Experimental Protocol

Each procedure started with calibration of the sensors for the markers locations on the subject's body, which included seven movement types: elbow flexion-extension, elbow supination-pronation, wrist flexion-extension, wrist abduction-adduction, shoulder flexion-extension, shoulder pronation-supination, and shoulder abduction-adduction. A static calibration was performed for the 4 targets positions and for the chair. Subjects were instructed to perform a reach to grasp to the targets, based on a visual signaling. They were requested to rest between the sets and allowed to rest when needed between trials. Two sets of 40 trials (10 trials per target, fixed random order) were recorded for a total of 80 movements per subject. The order of the sets was counter-balanced between subjects.

5.2.4. Analysis

Movements were determined as erroneous in several cases: there was a recording failure, the experimenter noted during task execution that the subject did not wait after grasping the cone, the target was misplaced, the experimenter determined that the subject did not perform the task well, or the error was identified during segmentation.

Movement trajectories were filtered using a Butterworth filter with 6 Hz cutoff frequency. The filtered profiles were used for determination of motion onset and offset. Tangential velocity was computed by differentiating position samples. Motion onset and offset were defined as the times at which the wrist (forward arm sensor) tangential velocity exceeded and remained above, or decreased and remained below 10% peak wrist tangential velocity. Hand closure was defined as the time at which the hand angular velocity decreased below 1% the hand peak angular velocity. The threshold was iteratively increased by 1% in case a hand closure was not identified. The segmentation was performed semi-autonomously. An automatic procedure was developed for initial segmentation and the segmentation results were all manually screened (Figure 5.4).

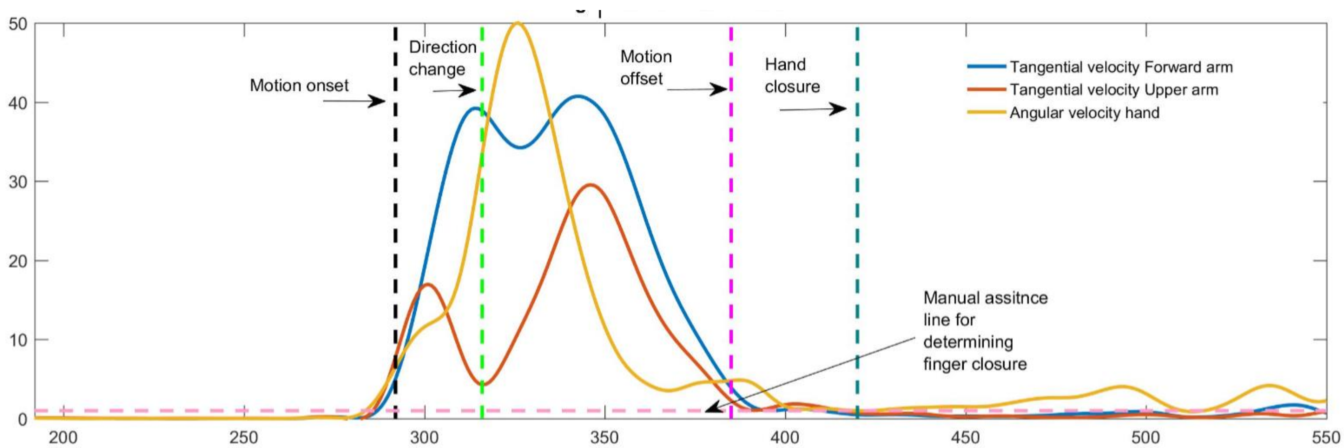

Figure 5.4: Segmentation analysis graph

The wrist configurations, were based on the recording of the distal arm sensor (sensor 2). For each subject, the configurations for all targets were translated to a unified, target centered coordinate frame origin, based on target location, recorded during the calibration phase.

Two data sets were formed, one for each group (stroke and healthy). A grasp affordance was estimated for each group based on the method detailed in chapter 3. The parameters were defined according to table 8.

5.3. Results

Out of 996 reach-to-grasp movements of healthy subjects, 941 were used (94.5%) and 55 erroneous movements were discarded. The number of movements per target are NC=237, FC=239, FL=234 and FR= 231. Out of 863 reach-to-grasp movements of patients with stroke, 829 were used (96.1%) and 34 erroneous movements were discarded. The number of movements per target are NC=204, FC=210, FL=211 and FR= 204.

5.3.1. Grasp affordance density of healthy subjects

The algorithm converged very fast after about 100 samples. The affordance densities established, includes two clusters (Figure 5.5-5.7, table 11). The two cluster positions are very close with a Euclidian distance of 2.6 inches. The orientation distinctly differs between the clusters, the mean vectors are 43.3 degrees apart. The composition of clusters by target is presented in Figure 5.7.

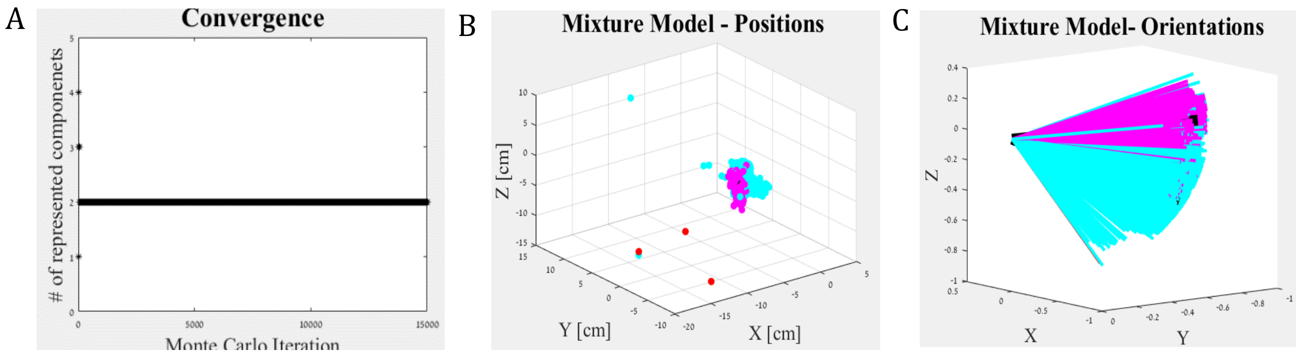

Figure 5.5: Healthey subjects- convergence and mixture model

Quaternions and positions are colored according to the cluster they are allocated to. The red colored data points above form a cluster weighing less than 5%.

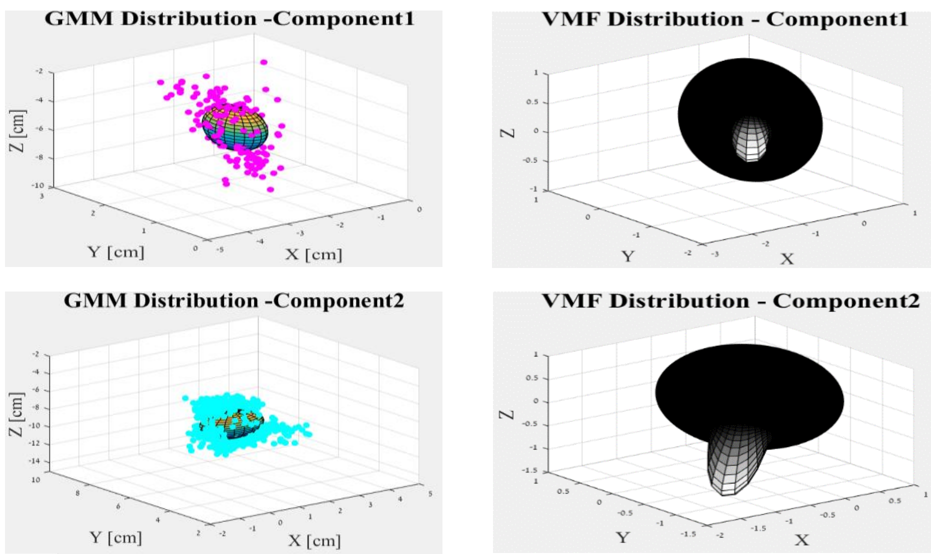

Figure 5.6: Healthy subjects- distributions by cluster

The center of the ellipsoid represents the expected value and the circumference is one standard deviation away from the center.

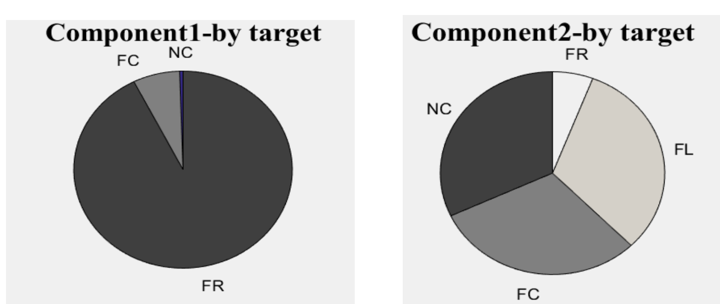

Figure 5.7: Healthy subjects- Component composition by target

TABLE 11: Healthy subjects- mixture model parameters

Cluster	1	2
Weight	0.215	0.782
Position		
μ	[-2.86,1.18,-4.74]	[-0.82,2.71,-5.01]
S	0.33,0.18,-0.29 0.18,0.26,0.07 -0.29,0.07,2.03	1.05,-0.06,-0.32 -0.06,0.43,0.42 -0.32,0.42,2.33
Orientation		
Kappa	99.74	57.52
μ_{cyc}	[0.881,0.164,0.266,0.3550]	[0.89,-0.166,0.114,0.409]

5.3.2. Grasp affordance density of patients with stroke

The algorithm converged after about 2000 iterations (Figure 5.8A). The convergence graph displays only clusters with a weight larger than 5%. The affordance densities established, includes two clusters (Figure 5.8-5.10, table 12). The two cluster positions are with a Euclidian distance of 5.1 inches. The orientation distinctly differs between the clusters, the mean vectors are 156.5 degrees apart. The composition of clusters by target is presented in Figure 5.10. Each subjects' dominant cluster and affected side are presented in table 13.

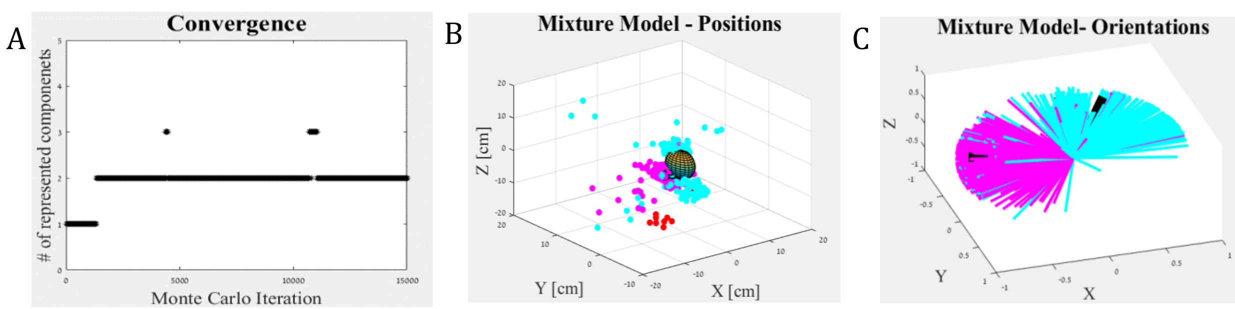

Figure 5.8: Patients with stroke- convergence and mixture model

Quaternions and positions are colored according to the cluster they are allocated to. The red colored data points above form a cluster weighing less than 5%.

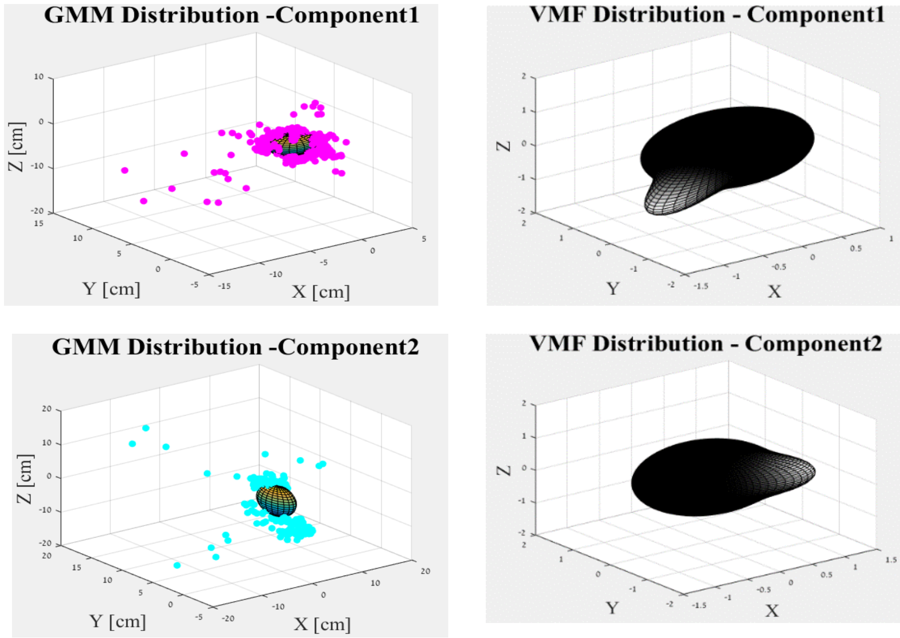

Figure 5.9: Patients with stroke - distribution by component

The center of the ellipsoid represents the expected value and the circumference is one standard deviation away from the center

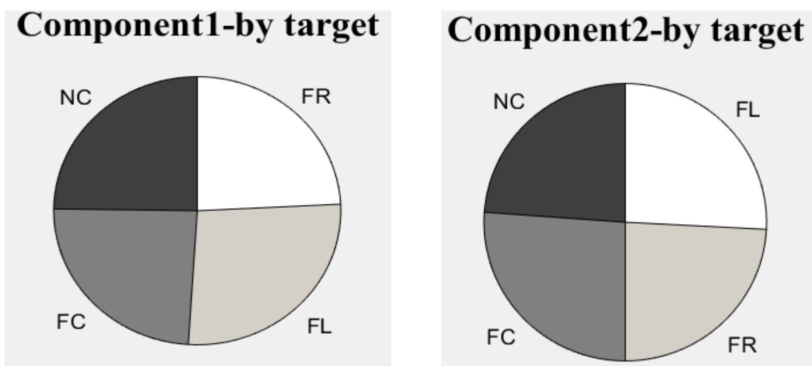

Figure 5.10: Patients with stroke- Component composition by target

TABLE 12: Patients with stroke- mixture model parameters

Cluster	1	2
Weight	0.53	0.46
Position		
μ	[-0.66, 2.44, -3.79]	[0.18, 0.91, -0.04]
S	4.65, -0.9, -0.79 -0.9, 2.94, 2.18 -0.79, 2.18, 5.58	4.23, 0.43, 2.86 0.43, 6.85, 8.11 2.86, 8.11, 20.83
Orientation		
Kappa	21.22	9

μ_{cyc}	[0.876,-0.17,0.047,0.45]	[0.964,0.045,0.071,-0.252]

TABLE 17: The dominant cluster of patients with stoke

Subject	Cluster 1	Cluster 2	Dominant Cluster	Affected Side (R-right, L-left)
1	65	10	1	R
2	3	57	2	L
3	31	7	1	R
4	4	68	2	L
5	33	2	1	R
6	0	44	2	L
7	1	79	2	L
8	55	9	1	R
9	0	10	2	L
10	2	78	2	L
11	42	1	1	R
12	69	10	1	R
13	38	2	1	R
14	48	1	1	R
15	47	4	1	R

5.4. Discussion

The affordance models of both the healthy subjects and patients with stroke are both composed of two clusters. However, the division of configurations between clusters is very different in the two models.

For the healthy group, the position Euclidian distance between the clusters of 2.6 inches, and orientation expected value difference of 43.3 degrees demonstrate a division between the clusters, hence, different grasp types. Grasp wrist configuration to three targets (FL, NC and FC) were allocated to the same cluster of the affordance density. The subjects used different configurations to the fourth target, (FR), and these were allocated to the second cluster of the affordance density. The division of clusters by target indicates there are different motion profiles executed towards different targets, this could be due to the different trajectory profiles. The variance in the data, both for orientation and position, is relatively small (concluded based on naked-eye observation (Figure 5.5) because calculating the exact variance of the data will not incorporate division to clusters and may be misleading). The small variance expected is reflected in the estimated model, cluster one: (σ_x^2=0.3, σ_y^2=0.3, $\sigma_z^2 = 2.03$, kappa=99.7) cluster two: ($\sigma_x^2 = 1$, $\sigma_y^2 = 0.4$, $\sigma_z^2 = 2.3$, kappa=57.5). Making it relatively easy for the algorithm to distinguish between the different grasps.

The affordance density of the stroke group was also composed of two clusters, (position Euclidian distance of 5.1 inches and orientation expected value difference of 156.5 degrees indicate a distinct division between the clusters. However, unlike in the healthy affordance density, the clusters are not divided by targets. Both clusters were composed of all targets' samples (FL, NC, FC and FR). Instead subjects were divided between clusters based on the hand with which they performed the movement (their effected arm). The variance in the data, both for orientation and position, is relatively high (naked-eye observation, Figure 5.8). the high variance expected is reflected in the estimated model, cluster one: (σ_x^2=4.7, σ_y^2=2.9, σ_z^2 =5.6, kappa=21.2), cluster two: (σ_x^2=4.2, σ_y^2=6.9, σ_z^2 =20.8, kappa=9). It seems the stroke group had the same grasp type regardless of the target's location.

6. **Bibliography**

Banerjee, Arindam. 2005. “Clustering on the Unit Hypersphere Using von Mises-Fisher Distributions” 6: 1345–82.

Bangert, Mark. 2010. “Using an Infinite von Mises-Fisher Mixture Model to Cluster Treatment Beam Directions in External Radiation Therapy.”

Bennis, Nezha, and Mindy F Levin. 2003. “H and Orientation for Grasping and Arm Joint Rotation Patterns in Healthy Subjects and Hemiparetic Stroke Patients” 969: 217–29.

Berenson, Dmitry, Siddhartha S. Srinivasa, Dave Ferguson, Alvaro Collet, and James J. Kuffner. 2009. “Manipulation Planning with Workspace Goal Regions.” *2009 IEEE International Conference on Robotics and Automation*, 618–24. doi:10.1109/ROBOT.2009.5152401.

Carr, Janet H., and Roberta Shepherd. 1998. *Neurological Rehabilitation*.

Casella, George, and Edward I. George. 1992. “Explaining the Gibbs Sampler.” *The American Statistician* 46 (3): 167–74. doi:10.1080/00031305.1992.10475878.

de Finetti, Bruno. 1995. “The Logic of Probability.” *Philosophical Studies* 77 (1): 181–90. doi:10.1007/BF00996317.

Desmurget, Michel, Claude Prablanc, and Claude Prablanc. 1997. “Postural Control of Three-Dimensional Prehension Movements.”

Detry, R., E. Başeski, M. Popović, Y. Touati, N. Krüger, O. Kroemer, J. Peters, and J. Piater. 2009. “Learning Object-Specific Grasp Affordance Densities.” *2009 IEEE 8th International Conference on Development and Learning, ICDL 2009* 2 (1): 1–17. doi:10.1109/DEVLRN.2009.5175520.

Dhillon, Is, and Suvrit Sra. 2003. “Modeling Data Using Directional Distributions.” *… of Computer Sciences. University of Texas …*, 1–21.

Eizicovits, Danny, and Sigal Berman. 2014. “Efficient Sensory-Grounded Grasp Pose Quality

Mapping for Gripper Design and Online Grasp Planning." *Robotics and Autonomous Systems* 62 (8). Elsevier B.V.: 1208–19. doi:10.1016/j.robot.2014.03.011.

Ferguson, Thomas S. 2014. "The Annals of Statistics," 5 (6): 1055–98.

Gelman, Andrew, John Carlin, Hal Stern, David Dunson, and Aki Vehtari. 2014. *Bayesian Data Analysis (Vol. 3)*.

Granville, Charles De, Andrew H Fagg, and Joshua Southerland. 2006. "Learning Grasp Affordances Through Human Demonstration," 1–6.

Itti, Laurent, Christof Koch, and Ernst Niebur. 2010. "Assessing a Mixture Model for Clustering with Integrated Completed Likelihood." *IEEE Transactions on Pattern Analysis and Machine Learning* 32 (11): 1899–1906. doi:10.1109/TPAMI.2012.125.

Jung, Sungkyu. 2009. "Generating von Mises Fisher Distribution on the Unit Sphere (S 2)," no. 1: 1993–94.

Lavalle, Steven M. 2006. "Sampling-Based Motion Planning." *Planning Algorithms*, 185–248.

Liebermann, Dario G, Mindy F Levin, Joseph Mcintyre, and Patrice Tamar L Weiss. 2010. "Healthy Subjects and Stroke Patients," 5242–45.

Lin, Keh-chung. 2008. "Effects of Modified Constraint-Induced Movement Therapy on Reach-to-Grasp Movements and Functional Performance after Chronic Stroke." *Clinical Rehabilitation*. doi:10.1177/0269215507079843.

Mandel, Michael. 2005. "Implementing the Infinite GMM," 0–4.

Michaelsen, Stella Maris, Ruth Dannenbaum, and Mindy F Levin. 2005. "Task-Specific Training With Trunk Restraint on Arm," 186–93. doi:10.1161/01.STR.0000196940.20446.c9.

Murphy, Kevin P. 2007. "Conjugate Bayesian Analysis of the Gaussian Distribution" 0 (7). doi:10.1.1.126.4603.

Neal, Radford M . 2003. *Slice Sampling*. *The Annals of Statistics*. Vol. 31.

Orloff, Jeremy, and Jonathan Bloom. 2014. Comparison of frequentist and Bayesian inference 1–7.

Posada, David, and Thomas R Buckley. 2004. "Model Selection and Model Averaging in Phylogenetics: Advantages of Akaike Information Criterion and Bayesian Approaches over Likelihood Ratio Tests." *Systematic Biology*. doi:10.1080/10635150490522304.

Press, James S. 2002. *Subjective and Objective Bayesian Statistics Second Edition*.

Rasmussen, Carl E. 2000. "The Infinite Gaussian Mixture Model." *Advances in Neural Information Processing Systems 12*, 554–60.

Reshef, Roi, Danny Eizicovits, and Sigal Berman. 2014. "Path Planning of Grasp-Aimed Robotic Tasks Using Rapid-Exploring Random Trees." *Proceedings of the Second RHEA International Conference on Robotics and Associated High-Technologies and Equipment for Agriculture*.

Reynolds, Douglas a. 2008. "Gaussian Mixture Models." *Encyclopedia of Biometric Recognition* 31 (2): 1047–64. doi:10.1088/0967-3334/31/7/013.

Roby-Brami, A., S. Fuchs, M. Mokhtari, and B. Bussel. 1997. "Reaching and Grasping Strategies in Hemiparetic Patients" 1: 1997.

Schwarz, G. 1978. "Estimating the Dimension of a Model." *The Annals of Statistics* 6 (2): 461–64.

Shalizi, Cosma Rohilla. 2016. "From an Elementary Point of View."

Thrasher, T Adam, Vera Zivanovic, William Mcilroy, and Milos R Popovic. 2008. "Rehabilitation of Reaching and Grasping Function in Severe Hemiplegic Patients Using Functional Electrical Stimulation Therapy." doi:10.1177/1545968308317436.

Torbati, Amir Hossein Harati Nejad, Joseph Picone, and Marc Sobel. 2013. "Speech Acoustic Unit Segmentation Using Hierarchical Dirichlet Processes." *Interspeech*, 637–41. http://dblp.uni-trier.de/db/conf/interspeech/interspeech2013.html#TorbatiPS13.

Xu, Lei, and Michael I. Jordan. 1996. "On Convergence Properties of the EM Algorithm for Gaussian Mixtures." *Neural Computation* 8 (1): 129–51. doi:10.1162/neco.1996.8.1.129.

Xu, Lei, Michael I. Jordan, and Geoffrey E. Hinton. 1994. "An Alternative Model for Mixtures of Experts." *Nips*, no. 7: 633–40.

Yang, Ming-Hsuan, and Narendra Ahuja. 1998. "Gaussian Mixture Model for Human Skin Color and Its Applications in Image and Video Databases." *Its Application in Image and Video Databases." Proceedings of SPIE* 3656 (January): 458–66. doi:10.1117/12.333865.

Appendix 1: Synthetic data sets

The synthetic data sets were generated using the random mixture model sampling algorithm developed (4.2.1). The synthetic validation set - distinct separation in both orientation and position was generated using table A.1. The synthetic overlap in position dataset (OP) was generated using table A.2. The synthetic overlap in orientation dataset (OO) was generated using table A.3 and synthetic overlap in position and orientation dataset (OPO) was generated using table A.4

TABLE A.1: Total separation- original model

Cluster	1	2	3
Weight	0.33	0.33	0.33
Position			
μ	[200,200,200]	[100,100,100]	[1,1,1]
S	1,0.1,0.1 0.1,1,0.1 0.1,0.1,1	1,0.1,0.1 0.1,1,0.1 0.1,0.1,1	1,0.1,0.1 0.1,1,0.1 0.1,0.1,1
Orientation			
Kappa	200	200	200
μ_{cyc}	[0,0.707,0.707,0]	[0,1,0,0]	[0,0,0.707,0.707]

TABLE A.2: Position overlap-original model

Cluster	1	2	3
Weight	0.33	0.33	0.33
Position			
μ	[0,0,0]	[3,3,3]	[6,6,6]
S	3,0.1,0.1 0.1,3,0.1 0.1,0.1,3	3,0.1,0.1 0.1,3,0.1 0.1,0.1,3	3,0.1,0.1 0.1,3,0.1 0.1,0.1,3
Orientation			
Kappa	200	200	200
μ_{cyc}	[0.462,0.191,-0.845,-0.191]	[0.733,0.462,-0.191,0.462]	[0.854,0.354,0.354,-0.1460]

TABLE A.3: Orientation overlap- original model

Cluster	1	2	3
Weight	0.33	0.33	0.33
Position			
μ	[1,1,1]	[10,10,10]	[20,20,20]
S	1,0.1,0.1 0.1,1,0.1 0.1,0.1,1	1,0.1,0.1 0.1,1,0.1 0.1,0.1,1	1,0.1,0.1 0.1,1,0.1 0.1,0.1,1
Orientation			
Kappa	50	50	50
μ_{cyc}	[0.707,-0.707, 0, 0]	[0,-1,0,0]	[0.854,0.354,-0.354,0.146]

TABLE A.4: Total overlap- original model

Cluster	1	2	3
Weight	0.33	0.33	0.33
Position			
μ	[0,0,0]	[3,3,3]	[6,6,6]
S	3,0.1,0.1 0.1,3,0.1 0.1,0.1,3	3,0.1,0.1 0.1,3,0.1 0.1,0.1,3	3,0.1,0.1 0.1,3,0.1 0.1,0.1,3
Orientation			
Kappa	50	50	50
μ_{cyc}	[0.707,-0.707, 0, 0]	[0,-1,0,0]	[0.854,0.354,-0.354,0.146]

Appendix 2: Demographic data

Demographic data of subjects with stroke and healthy control subjects are presented in table A.5 and table A.6 respectively.

TABLE A.5: Subject with stroke- demographic data

	Age (Years)	Country	Gender	Effected Side (R-Right, L-Left)
1	59	IL	F	R
2	46	IL	M	R
3	62	IL	M	R
4	66	CA	M	L
5	46	IL	M	R
6	38	CA	M	L
7	50	CA	F	L
8	77	IL	M	R
9	54	IN	M	R
10	71	IN	M	R
11	50	IN	M	L
12	62	IL	F	R
13	59	IN	F	R
14	48	IN	F	L
15	57	IL	F	R
	Mean 57.4			
	SD 10.9			

TABLE A.6: Healthy subjects- demographic data

	Age (Years)	Country	Gender	Hand used (R-Right, L-Left)
1	57	IL	M	R
2	57	IL	F	R
3	50	IL	M	R
4	52	IL	M	R
5	65	IL	F	R
6	72	IL	F	R
7	54	IL	M	R
8	55	IL	M	R
9	50	IL	M	R
10	66	IL	F	R
11	76	IL	M	R
12	62	IL	M	R
13	70	CA	M	R
	Mean 60.4			
	SD 8.5			

תקציר

אחיזה ותמרון של אובייקטים בסביבה סבוכה ולא מובנית היא משימה מאתגרת עבור בני אדם ומערכות רובוטיות. אחד המרכיבים ההכרחיים לאחיזה מוצלחת הוא המיקום והאוריינטציה (קונפיגורציה) של מפרק כף היד, שמהם האובייקט נאחז. קביעת קונפיגורציה לאחיזה הינה חלק אלמנטרי מתהליך תכנון התנועה של הושטה אל עבר אחיזה reach-to-grasp). צפיפות התפלגות אחיזות מוצלחות (grasp affordance densities) הינן פונקציות התפלגות מרחביות המייצגות הסתברויות לאחיזה מוצלחת של מפרק כף היד מסביב לאובייקט. על מנת לייצג את המיקום ואת האוריינטציה בצורה מתאימה, פונקציית ההתפלגות צריכה להיות מבוססת על מודל מעורב (mixture model) שמשלב רכיבים עם התפלגויות ציקליות ולא-ציקליות. אנחנו פיתחנו שיטת שיערוך בייסיאני לא פרמטרי, אשר מתאימה עבור רכיבים עם התפלגויות מעורבות, הרכיבים מורכבים מהתפלגויות התפלגויות גאוסיאניות (Gaussian) וון מיסס פישר (Von Misses-Fisher). שערוך בייסיאני, לא פרמטרי, מאפשר שיערוך של מספר הרכיבים וערכם של הפרמטרים במודל מעורב. בנוסף, השערוך הבייסיני, שלא כמו שיערוך המבוסס על נראות מקסימאלית, פחות מועד לתופעות של התאמת יתר ומינימום מקומי מאלגוריתמים מבוססים נראות מקסימאלית. האלגוריתם שפותח משולב עם אלגוריתם תכנון תנועה אל עבר אחיזה רובוטי ועבור ניתוח תנועה של חולי שבץ. עבור האלגוריתם תכנון תנועה של הושטה אל עבר אחיזה, הרובוטי, שילבנו את שערוך צפיפות התפלגויות עם אלגוריתם תכנון התנועה bi directional Ranomly Exploring Random Trees (RRT). האלגוריתם שפותח (GA-RRT) , grasp affordance RRT מספק מספר רב של קונפיגורציות מטרה עם הסתברות גבוהה לאחיזה טובה. האלגוריתם GA-RRT נבדק בסימולציה עבור תכנון תנועה לאחיזת ספל בחמש סביבות עם מכשולים. בסביבה אחת האלגוריתם לא מצא קונפיגורציית מטרה מתאימה, מכיוון שהסביבה היתה סבוכה במכשולים וכדי להגיע אל האובייקט נדרש להגיע לאוריינטציות שלא נכללו בבסיס הנתונים המקורי שממנו ההתפלגות שוערכה. בארבע הסביבות האחרות, 95% מהדגימות הובילו לאחיזות טובות. האלגוריתם שפותח יושם על מנת לשערך צפיפות התפלגויות אחיזות מוצלחות ל- 15 חולי שבץ ו - 13 נבדקי בקרה, מותאמי גיל, בריאים. נבדקים בשתי הקבוצות ביצעו תנועה של הושטה על עבר אחיזה למטרות בארבעה מיקומים. צפיפות התפלגות אחיזות מוצלחות שוערכו עבור כל קבוצה. עבור כל אחת מהקבוצות עם הנתונים מכל המטרות יחדיו. עבור שתי הקבוצות, צפיפות התפלגות כללו שני רכיבים, אך סיבת החלוקה לרכיבים הינה שונה. עבור קבוצת הנבדקים הבריאים, הקונפיגורציות של שלוש מטרות שויכו לרכיב אחד והקונפיגורציות של המטרה הנוספת שויכה לרכיב נפרד. עבור קבוצת חולי השבץ, החלוקה לרכיבים התבצעה לפי היד הפגועה, שבה ביצעו את התנועה. בנוסף, השונות בתוך הרכיבים הייתה גבוהה יותר עבור הקבוצה של חולי השבץ.

מילות מפתח: שערוך בייסיאני לא פרמטרי, צפיפות התפלגות אחיזות מוצלחות, מודל גאוסיאני מורכב, התפלגות וון מיסס פישר, אחיזה, תכנון תנועה, שבץ.

אוניברסיטת בן גוריון בנגב

הפקולטה למדעי ההנדסה

המחלקה להנדסת תעשיה וניהול

שערוך בייסיאני של פילוג קונפיגורציות מרחביות

חיבור זה מהווה חלק מהדרישות לקבלת תואר מגיסטר בהנדסה

מאת: רותם דואני

מנחה: פרופ' סיגל ברמן

חתימת המחבר:... תאריך:.................

אישור המנחה:... תאריך:.................

אישור יו"ר ועדת תואר שני מחלקתית:...................................... תאריך:.................

תשרי תשע"ז אוקטובר 2017

אוניברסיטת בן גוריון בנגב

הפקולטה למדעי ההנדסה

המחלקה להנדסת תעשיה וניהול

שערוך בייסיאני של פילוג קונפיגורציות מרחביות

חיבור זה מהווה חלק מהדרישות לקבלת תואר מגיסטר בהנדסה

מאת: רותם דואני

תשרי תשע"ז

אוקטובר 2017